Response to reviewers

Reviewer 1

We thank to reviewer 1 for the positive comments on our manuscript.

Reviewer 2 (G. Kwiatek)

We would like to thank to G. Kwiatek for his thorough review, which we led to great improvement of the manuscript. We were able to address almost all of his comment as detailed below.

The Authors put a lot of efforts in constraining the hypocenters of AE activity. However, I am puzzled why they did not use the S-waves to improve the location quality? From Figure and the paper itself it is clear the S-waves were efficiently recorded and they could help to constrain the locations. S-phases have been applied in previous studies using similar acquisition system with success (JAGUARS project, ASPO FHF experiment, see appropriate papers). Could you comment on that and also inform the Readers on your choices?

Although in many events the S-waves are clearly discernible, we found that the onset times of only a few of them could be accurately picked, while most of them are associated with considerable uncertainty. Furthermore, the S-wave velocity of the rock mass is not well described in the literature, and our S-wave arrival times are too few to determine a reliable S-wave velocity model. For these reasons, and the fact that the locations are already well determined with P-wave arrivals only, we decided that the effort to pick and use S-waves arrival is more trouble that it is worth.

In introduction (L145-149) I think it would be fair and beneficial to mention in this context a concurrent Aspo FHF experiment (Zang et al., 2017; also: Kwiatek, G., Martínez- Garzón, P., Plenkers, K., Leonhardt, M., Zang, A., Specht, S., Dresen, G., and M. Bohnhoff. Insights into complex sub-decimeter fracturing processes occurring during water-injection experiment at depth in Äspö Hard Rock Laboratory, Sweden, JGR, submitted, or equivalently a similar, but already published contribution at the Schatzalp workshop on Induced Seismicity). The aim of ASPO experiment was to optimize the hydraulic fracturing procedure and limit the occurrence of undesirable LME. Otherwise it seems your introduction is incomplete.

We included the proposed references in the introduction.

The calculation of average cross-correlation coefficient (L293-294) seems to be not conducted fully appropriately. The ensemble of correlation coefficients should be first transferred to the Fisher's domain (Z-domain) and then averaged. The resulting average can be transferred back to the "regular" domain by the inverse Z-transform (variance stabilizing transformation). Please correct.

We included the Fisher transformation in our cluster analysis procedure (also mentioned in now in the manuscript) and found comparable results to the previous analysis without the Fisher transformation. We updated Figure 8 and 9 with the new results and adjusted the text accordingly. As the events for which focal mechanisms were computed do not fall into the same clusters as before, we removed the grouping into events belonging to different clusters. The results and interpretations remain the same.

Regarding the observations related to shear/tensile events (L390-L392). I would definitely appreciate here more extensive presentation of results in exchange for the pure reference to Eaton's paper. What is the range of ES/EP energies (or S/P amplitudes) you observe? Do the observed values of ES/EP or S/P amp. ratio allow to suggest the existence of tensile components? (cf. discussion in Kwiatek, G. and Y. Ben-Zion (2013). Assessment of P and S wave energy radiated from very small shear-tensile seismic events in a deep South African mine. J. Geophys. Res. 118, 3630-3641, DOI: 10.1002/jgrb.50274.).

We expanded the short discussion on possible presence of tensile source components by giving the range of observed S/P-wave amplitude ratios, and mention that low values may point to a tensile component, as found by Kwiatek and Ben-Zion (2013) (added as reference).

In lines L473-L475: Stress rotations due to pressure changes were already reported for geothermal reservoir (Martínez-Garzón, et al., GRL, (2013), DOI: 10.1002/grl.50438) and also confirmed recently by synthetic modellings (see Ziegler et al., Schatzalp 2017). If you want to keep this section (see minor comments), that could benefit to the discussion.

We moved this section to the discussion section and added the suggested reference Martínez-Garzón, et al., (2013). We also added the earlier paper on stress perturbations due to hydraulic fracturing by Warpinski & Branagan, Altered stress fracturing, JPT,1998.

The comparison of stress estimations (_L530-532). I am really puzzled why the Authors did not perform the stress tensor inversion using the polarity data, e.g. following the nonlinear stress tensor inversion (MOTSI Abers/Gephart), and rely their results on the spatial orientation of the fault planes. I believe stress tensor inversion would provide additional information supporting your findings.

Stress inversion from polarization data is not the primary goal of this paper and may in fact produce very misleading results. Instead, we strive to obtain reliable orientations of the seismicity clouds that provide an indication to the σ3 direction, and to compare these to the results of other stress measurements. Clearly, the found focal mechanisms do not match well to the the stress field orientation estimates from both the seismicity clouds and the overcoring measurements. As discussed later, the focal mechanisms may indicate the stress perturbations around the propagating fracture, which in our case would invalidate the use of polarization data to infer stress orientations.

I am afraid I am not fully understanding your discussion on mechanisms (L570-580). Looking at your mechanisms the variability of the fault plane solutions does not seem extreme. Why don't you plot a Mohr circle and discuss how (even the composite) fault plane solutions fits to the stres field derived from other measurements. It may be that the fault planes (regardless of whether they are normal, strike slip or thrust) may actually be critically stressed in this complex environment. This was successfully applied for analyzing ASPO data (see Kwiatek et al., 2017, Schatzalp proceedings).

By plotting the stress conditions along the focal planes in a Mohr-Coulomb diagram, we indeed find that pressure leak-off is sufficient to explain the different focal mechanisms. We added such a figure to the text and adjusted the discussion on the topic accordingly. Thanks for the great idea.

Minor comments

L65 I understand that the volume is related to small-scale hydrofracturing projects. However, it would be good to write it down here once again explicitly to distinguish it from larger-scale industrial projects

Corrected.

L73 Naming convention for "microseismic" is not consistent. You either use microseismic or microseismic. Please unify.

We replace micro-seismic by microseismic throughout.

L83 Manthei

Corrected.

L124 Zang et al., 2017 (and everywhere else, the appropriate reference is: Zang, A., Stephansson, O., Stenberg, L., Plenkers, K., Specht, S., Milkereit, K., Schill, E., Kwiatek, G., Dresen, G., Zimmermann, G., Dahm, T., and M. Weber (2017), Hydraulic fracture monitoring in hard rock at 410m depth with an advanced fluidinjection protocol and extensive sensor array, Geophys. J. Int., 208(2), 790–813, DOI:10.1093/gji/ggw430)

Corrected.

L215 The Wilcoxon does not seem to work very efficiently above 17kHz (cf. appendix in Kwiatek et al., 2011) and our experience was that the transfer function was not flat above this range.

Corrected.

L217 You use "piezo-sensor", however the well-defined term in the field (cf. Kwiatek et al. 2011 and other follow-ups) is the "(in-situ) acoustic emission sensor" or simply "acoustic emission sensor".

We prefer to keep this term (that is also used in other articles) as we feel it is less ambiguous. Acoustic emission in our understanding refers to a target frequency band. Thus, the term 'acoustic emission sensor' does not say anything about the sensor technology; both piezosensors and accelerometers may be called 'acoustic emission sensors' as they can cover the acoustic frequency range.

L226 SBH-1

Corrected throughout.

L229-230 This is in surprising agreement with what was observed at ASPO FHF (reference?)

I did not find such an observations stated by Zang et al., 2017 or any other ASPO reference.

L244 Correct the reference

Corrected.

L251 How the P-wave velocity was estimated (any details, reference, variability?)

We already describe that the P-wave velocity model is estimated using a grid-search approach minimzing the differences between observed and predicted P-wave arrival time. We feel the information given is already appropriate

L279-L284 It is not clear what this procedure reflects. Are you concerned about velocity mismodelling, or P-wave mispicking. Please clarify.

We now clearly indicate in the manuscript that we are concerned with P-wave arrival time uncertainties.

L286 Is it 95% confidence interval?

Yes. We added this in the manuscript.

L323-325 This is similar to what has been observed at ASPO, please refer.

We added reference to Zang et al., 2017.

L357-L385 The sentence starting with "Clear rings..." is not understandable, please rephrase/modify/extend it.

We formulate this statement more clearly now.

L380 all 112

Corrected.

L411 npi f_0

Corrected.

L412 P-wave

Corrected.

L413 What is the range of dominant frequencies you have and how this correspond to the resonant frequencies of the AE sensors? Does it not lead to overestimation of magnitude, as you enhance the resonances at high frequencies due to Q correction?

The range of dominant frequencies is between 1 – 10 kHz as not indicated in the manuscript. To avoid artificial enhancement at (currently unknown) sensor resonance frequencies, we follow the recommendation of Zang et al., (2017) and filter data between a narrow band-pass filter between 3 and 7 kHz and use nominal frequency f_0 = 5 kHz to correct for attenuation.

L420 Unfortunately to the project, this suggest putting accelerometer sensors on tunnel walls does not allow to effectively record such small seismic events despite of reasonable source-receiver distances.

Although we agree that this might be the case, it does not naturally conclude from our study, as we did not compare borehole versus tunnel wall installation of accelerometers. Thus, we refrain from commenting on this in the manuscript.

L425 This part is hard to understand. Please refer to exact figures. The caption of figure 10 is poor - it is hard to understand differences between a) and b) (stress drop...), Please explain all the details of the figure in the caption!!!

We expanded the caption with details so that figure 10 and caption become self-explanatory. We also improved the details of this computation in the manuscript.

L426 Guess there is a typo here. I have no idea how you calculated so small source radii for the assumed stress drops of 1MPa. Using Eshelby's formula bring me to way larger values of the order of meters (0.8-2.5m i.e. 80 to 260 cm, not 8 to 25 cm as you write) for the stress drop of 1MPa. Anyway, calculations for 0.1MPa seems to be fine. It is also more reasonable assumption regarding the frequencies and expected source radii as well as the low expected confining pressure (stress drop seems to be dependent on average stress)

Indeed, we must have made an error in the calculations. The source radii lie between 1.4 and 4.3 meter for stress drop of 1 MPa and 0.3 – 0.9 m for 0.1 MPa stress drop. We changed the numbers in the text and figure 10 as well as the corresponding discussion accordingly.

L440 What is the b-value? Is it comparable with what is observed for other fracking project (high values)?

Due to the limited number of events with magnitudes and associated high uncertainty in b-value computation, we decided to report only report a robust lower bound for b-values that is estimated to be >2.

L453 Isn’t it simply the composite fault plane solution?

Due this and the following comment we decided to remove these focal mechanisms based on stacked waveform polarizations.

L460-L461 I think it is over-intepretation. I guess if you stack multiple double-couple sources with even slightly different focal mechanisms you may achieve spurious non-DC components (e.g. Frohlich, 1994). Therefore, i am not sure if your reasoning do not go to far. I guess waveform stacking is not the way you can get a reasonable message with respect to the mechanism of faulting (shear/tensile). Please reduce L455-L465 to solid observables and reduce the discussion.

We agree with the reviewer that this is possibly beyond any reasonable interpretation, as it is not clear what such ‘stacked focal mechanisms’ represent. We therefore remove them from Figure 11 and the corresponding text in the manuscript, and thank the reviewer for pointing out a reference that has already considered the problem.

L467-L475 This paragraph should go to discussion, if you are concerned about the (apparent) lack of non-DC events. I am not concerned and I do support your findings, though, and believe your results are solid without too much speculations on why you don’t observe tensile openings. As you write, the tensile openings are energetically ineffective, and likely limited to the very small earthquakes that likely cannot be handled properly by AE system.

We agree and moved the paragraph to the discussion, where parts of it are repeated anyway (we kept the first sentence as it goes well with the end of the previous paragraph). We also included the reference to Martinez-Garzon et al., (2013) that was recommended earlier.

L493 Nice observation

Thanks!

L500 Some crossed-out words

Corrected.

L530-532 Some more crossed-out words

Corrected.

L559 Stress magnitudes and stress field should be presented earlier in the manuscript
(just before section 3 i suggest)

We moved the table with the stress information to the end of the section on stress measurement.

L594 "readily be applied to failure at such scales"? Is that what really want to write?

We changed the sentence to ‘can be applied to seismicity at such scales’

Figure 2 "d)" is misplaced. The idea of coloring per HF is a good one, but the problem is you re-use these colors for painting other curves (e.g. Injection pressure and rate in Figure 2). Maybe it is possible to take advantage of other colors or patterns (e.g. dashed lines) in this and other figures while you NOT refer to the particular stimulation. Finally I suggest to repeat HF# label in each panel and also paint dots in g,h,i with appropriate color reflecting HF.

We improved the figure as suggested by the reviewer.

Figure 4. Hard to read... Why not to put simply a 2D version of this plot (e.g. view from top)?

A 2D plot would conceal the borehole seismic array, which nicely shows the impact of the anisotropy on station corrections. Indeed the 3D view is difficult to read, however, we could not find a better view angle.

Figure 6. Mark HF1 HF2 and HF3 labels in a). I suggest to change colors in b) to not confuse reader with what is in the subplot a)

Changed as suggested.

Figure 10. Please rewrite the whole caption. The content of the figure is quite badly explained. What is R? Please enhance stress drop messages, or just explain in caption what is the difference between a) and b) subplot.

We changed the figure and caption accordingly and added more information (see comment further up).

Figure 11. Remove "for a few events". I suggest to put shading to distinguing thrust from normal focal mechanisms more easily.

Caption changed as suggested. We feel the focal mechanisms are more clear without shading.

Reviewer 3 (Enrico Caffagni)

Major concerns

1. The Abstract is quite long in comparison to standard EGU Discussions abstracts.

We shortened the abstract by removing the information on fracture initiation at the borehole wall that was probably driven by strength anisotropy, which is not a major overall scope of the paper.

2. The Discussion can be shortened, avoiding repetitions of concepts.

We have already shortened the discussion somewhat in response to reviewer 2. However, we feel that there are many aspects of fracture growth that is noteworthy and that we would like to discuss. Thus, we also added a short paragraph discussing the unidirectional fracture growth (referring to Dahm et al., 2010) as suggested by the reviewer further below.

3. Some references are missing or written in an incorrect way.

We corrected this.

4. Table 2 is present, but never mentioned in the text.

We added reference to Table 2

5. Figure 11 appears with overlapped labels.

Corrected.

6. I feel that a bit of clarification is needed when the authors described the "Microseismic monitoring". I think it is more a question of terminology. The classical induced microseismic events range in frequency between 80 to 300-400 Hz. No more. Sure that the space-time scale is different. Yet you measure events at magnitude -2.5 for instance at KHz. Should we define these as "acoustic emissions"? You actually mention, page 6 line 208-209, "similar to those commonly used in laboratory acoustic emission". For coherency, you should continue to call such events as acoustic emissions, throughout the paper.

We are aware that typically high frequency seismic events are referred to as acoustic emissions. However, the distinction to seismic events is not clear and different frequency thresholds are given, above which events are supposed to be called acoustic emission. In fact, also events above ~20 Hz are audible and might be referred to as acoustic emissions. In our view, microseismic or just seismic is the more general term describing simply elastic waves. We thus prefer this term over acoustic emission.

7. I am not sure that your stress characterization study is in the 'far-field' domain, page 6 line 184, at least if this is only due to the "several tens of meter away from any fault". What you are doing, I believe, instead is a characterization of the "local" stress field. Which is more useful.

We agree that the term 'far-field' is misleading in this context. We changed the term to indicate that it is an estimate of the unperturbed (or less perturbed) stress field some distance away from the fault.

8. It would benefit your paper to include, at a qualitative way, one or two sentences on the topic: what drives the initiation of an hydrofracture, and "when" or "why" it decides to stop? I suggest to refer to Dahm et al. (JGR, 2010), who discuss the effect of the pore pressure gradient, or pressure gradient, which in your experiment might be also responsible of fracture plane deviation or the trend in

asymmetrical growth, page 16 line 544 better. Your pressure gradient might drive the fracture, but when this starts decreasing, well, your fracture "feels" the local stress field then re-orients itself naturally. Another plausible explanation of fracture plane rotation is a high resilient tectonic stress, see Cooke et al. (2016, TLE). (it is just an attempt of clarification; there are better interpretation; work on that)

The work by Dahm et al., (2010) is indeed a possible explanation for our asymmetric fracture growth (although possibly not a sufficient explanation). In case of the work by Cooke et al., (2016), we are not convinced that it is transferable to our case.

We added a section discussing the asymmetric fracture growth observed based on Dahm et al., (2016)

9. I honestly do not see a strong connection between polarization through stacking and focal mechanisms. In Figure 11 in a few beach-balls a few events appear in different color (black and white) yet in the same section of the ball. This seems to be contradictory. Actually, by itself, the stacking operations is for enhancing the signal arrival, not for polarization; unless one projects first the traces into already obtained polarization vectors then perform the stacking. By such methods one can locate microseismic events (see Caffagni et al. 2016, GJI).

We agree that the waveform stacking to retrieve better polarization analysis is problematic and have removed this from the text and the corresponding figure (also in response to reviewer 2).

Beside that, the lack in the majority of strike-slip events or a combination of different source mechanisms seems to be a kind of constant in induced seismicity. You can see and refer for instance to Baisch et al. (2015, BSSA; Figure 12).

Indeed, other authors have also observed focal mechanisms that deviate from the prevailing stress field, although in most of these cases (Baisch et al., 2015; Deichmann et al., 2014) the majority of the focal mechanisms does agree with the stress field.

We added a sentence mentioning these observations by other authors.

10. The authors need to be careful when they declare "the observation of DC components..exclude 1" page 17 line 577-578. No, I do not agree. A tensile source mechanism has a DC component as well. In addition Figure 8 reproduces what to me is a tensile event, Cluster 2 (max P wave is bigger than S wave). If I had to sort hundreds of events automatically and visually, I would classify that event as a tensile one.

We disagree on this comment, pure tensile sources do not have a DC component, otherwise they are not pure tensile sources as they require a shear component. Also, a P-wave that is stronger than the S-wave is not necessarily indicative of a tensile event: depending on where you are in the radiation pattern, the P-wave may be much stronger than the S-wave for a pure DC event (i.e. at 45° from the focal planes). In addition, the sensitivity to S- and P-wave in dependence of sensor orientation is not known. Generally, simple visual assessment of S to P-wave ratios may be misleading to distinguish DC from tensile sources; for this full moment tensor analysis is recommended, which is currently not possible with our data.

11. The authors mention in the Appendix, page 20 line 652, "a solid angle is also referred to as the takeoff-angle". The classical take-off-angle is not defined as a solid angle, see Stein and Wysession page 222.

We changed the wording to say that the solid angle is a function – or is representative - of the so-called take-off angle.

12. More than else, since you as ETH group are currently leading the laboratory experimental research of hydraulic fracturing in Europe, it would benefit to develop on the topic: What's for? Switzerland might be soon venue of massive usage of geothermal exploitation. What can we learn at macro-scale from such experiments at micro-scale? Can just we simply "upscale" our results in cases of real large-scale stimulations? Perhaps the answer is yes. Injection values in pressure are much higher though and perhaps the effect of small-scale rock anisotropy might vanishes in comparison to big deformations due to pore-elastic effects or fluid diffusion or fracturing.

The paper you want to publish is called "EGU Discussion". It would be appropriate if you could "unbalance" yourself and make some qualitative or even quantitative declarations on future perspectives from such mini-scale hydro-fracturing experiments.

As the reviewer has already indicated that the discussion is rather long, we prefer to refrain from expanding it towards possible implications for experiment several scales larger than our hydrofractures. Although we agree that various observations may have implications for the large reservoir scale, we prefer to discuss our observations at their scale and leave it to the reader to transport insights to the larger-scale.

In the following you will find my minor concerns. Please, do not reply in your response file to all of them. But make sure to read them and revise. I have also added additional important concepts missing.

Minor concerns

Abstract

Line 15: "transverse" to what? To the radial? Usually P-waves propagates in the radial direction

'Transverse isotropic' is a standard term in anisotropic elasticity theory. Transverse possible related to the symmetry axis.

Line 20: " from the overcoring stress. An anisotropic elastic model.."

We changed it to '...overcoring stress tests, provided an anisotropic …'. By adding a comma it becomes clear the second part after the comma belongs to the first part of the sentence.

Line 21 "sigma1 is significantly.." to Line 24 "the north". Is not clear and I would simply remove it, to shorten the abstract

The stress field characteristics described here are key outcomes of the paper. We prefer to mention it in the abstract. We shortened the abstract by removing aforementioned information (Comment 1 above)

Introduction

Line 37: "Hydraulic fracturing or hydrofracking (HF)"

We prefer to avoid the more colloquial term 'hydrofracking'.

Line 37: Rephrase "Hydraulic fracturing induces artificial fracture networks in a rock mass by highpressure fluid-injection. It has become an essential technique…, for instance to enhance the permeability…, and increase… . HF should not be confused with hydroshearing (HS). HS is a method of rock.. that uses fluid-injection….promoting shear failure, attendant dilation of pre-existing fractures, and fault slippage…"

We partially adapted the changes in the manuscript.

Line 45: “criticality of the discontinuity sets” What do you mean? It is not clear

We added ‘proximity to failure’ as explanation.

Line 47: “HS has been often exploited in… . HF small volume has been also utilized in stress..” I would replace the “deep geothermal projects” with the EGS, the “Enhanced Geothermal systems”

We use the acronyms as suggested and use enhanced geothermal systems.

Line 52: “etc; see Zang and...2010”

Changed.

Line 52: “To better constrain the stress field...and sections where no pre-existing fractures are present”

We prefer to keep our formulation for brevity.

Line 55: “water is injected at a constant rate until the ..down, initiating a fracture at the borehole wall...sub parallel to the principal…., and significant deviations are not expected due to the tensile strength anisotropy..” Is this what you mean with “no complications from tensile...” If not, please provide explanations.

Changed as suggested.

Line 57: “, then high-pressure fluid injected will tend to initiate an axial fracture” Is this what you mean? Is not clear what initiates the fracture.

Changed as suggested.

Line 59: “minimum principal stress is close to be aligned to the borehole axis”

Our formulation is correct.

Line 65: “Injection volumes..” You do not mention here the injection rate (in litres per minutes), which is one of the constraining factors as well of the induced seismicity.

We here refer to the size of the hydro-fracture, which is constraint be volume and not injection rate.

Line 67: “at which the breakdown occurs”

Changed.

Line 70: “treatments (of importance here) it can be considered as the pressure...open. ISIP is thus interpreted as...”

Changed partially as suggested.

Line 71: “intended for HF or HS, can generate acoustic emissions and microseismic events” (see my comment n. 6)

We prefer not to distinguish between acoustic emissions and microseismicity as the distinction is not clear.

Line 75: “regardless of scale” What scale? Time- space-scale?

We refer to the HF scale.

We added this in the text.

Line 76: “monitoring has been routinely used..” Check you references. They are all in the past. You cannot use the present tense.

Using the past is also not appropriate as microseismicity is still being used routinely.

Line 78: you may include: Caffagni et al. 2016

We added the reference.

Line 78: “At the other extreme of scale”. What scale?

We refer to the HF scale.

We added this in the text.

Line 84: “indicate changes in the local stress condition”

We prefer to keep our formulation as it is more complete.

Line 87: “controlled by..” Here you may develop on the pumped fluid, the pressure gradient (see Dahm et al. 2010, JGR)

Here we only discuss impact of stress field and anisotropy on fracture orientation. However, we later added in the discussion section a discussion asymmetric fracture growth that includes the interesting study by Dahm et al., (2010).

Line 94: “direction sigma 3 (Haering…,) particularly for HF operation (Rutledge…; Zoback et al. 2012 SPE)”

Changed as suggested.

Line 100: “Deichmann et al. 2014; Eaton and Caffagni, 2015, First Break)

We added the reference as suggested.

Line 107: “ Detailed moment tensor….have shown that most of the induced…with relatively a few...”

Changed partially.

Line 111: “is very inefficient in radiating” No. Energy from acoustic emissions is radiated efficiently but with a classical monitoring systems of geophones it is not detectable. Please correct.

We did not claim that acoustic emissions are inefficient in radiating energy, but tensile fractures. The notion is also supported by the fact that acoustic emissions mostly have double-couple sources, and only rarely are secondary opening components observed.

Line 113: “Thus,...do not necessarily...themselves, yet they contribute to illuminating the overall plane of fracture growth..”

We feel our formulation is more precise.

Line 117: “there are a few..between meter-scale….and the ambient stress..”

Changed as suggested.

Line 121: “though it would be desirable”

Our formulation is correct, too.

Line 135: “water injection” You mean the “injection history”? If so, please revise

Corrected.

Line 135: “Then, we detail our anisotropic...localization method.. The obtained results are then compared to the overcoring stress field observations” Is this what you mean?

Changed as suggested.

Line 164: “Since in-situ stress is a relevant factor driving...” you cannot say that is the “major force”, also the fluid-injection effects, e.g., pore pressure diffusion and propagation are important

Changed as suggested.

Line 176: remove “that serves”

Changed.

Line 178: “yields estimate of the full 3D stress”

Changed.

Line 184: “The goal is to characterize the local stress condition” see my comment n. 7

Changed accordingly.

Line 187-188: “It was intended...Pahl et al..” the meaning is clear. Rephrase with better English

We changed the sentence to make it clearer.

Line 196: “HTPF”. Never mentioned, please spell it

Corrected.

Line 209: “experiments” Include at least one reference

We added a reference.

Line 215: “accelerometers” remove the Italic format

Changed (also for piezoelectric sensors further above).

Line 231: “Signals were digitized with a 32-channel...” Is this what you mean?
Changed.

Line 237: What is the reason of this “dead-time”? Please provide a few explanation

We explain in brackets that this is related to the system being occupied to store the detected waveform.

Line 256: “this spans only 7 m” What you had in mind is the “array’s aperture”? If so, please revise

Changed.

Line 262: “transverse isotropy” Is this correct? Or it is instead “transverse anisotropy”? You mentioned before the elastic anisotropy approximation of Thompson..

Yes, ‘transverse isotropy’ is correct and a standard term in literature.

Line 282: “1000 time” Is this a peculiar number? Why not stopping the repetition at 100. What would happen? Please provide a few explanation. Also, what about the computational time? This would be important to reproduce the results.

We add a short explanation that 1000 repetitions yields a statistically representative sample.

Line 283: “principal component analysis” You can also include the accepted acronym “PCA”.

We prefer to spell out for clarity.

Also in this section, it might help the reader to see an image of your procedure, a visualization of your located clusters. You can decide to include an additional figure here. Also a number of questions raises up, such as are there events co-located? Did you identify repeated slips? You can provide a few explanation based on your results

We here limit ourselves to the method description, while the results on located clusters and repeated events are covered later.

Line 319: “due to the lower noise-levels in the borehole” Have you really checked in the traces if what you argued is true? If so, what are the noise levels or the signal-to-noise-ratio?

We indicate that the noise-level is less than half of the one from the tunnel sensors.

I would move Line 322-331 at the beginning of the Results section page 9. First you describe your HF treatment parameter, then you move to the induced seismicity description

We prefer to keep it as it is, as moving this section would compromise the text structure. We first describe general event statistics (number of detected/located events) and then describe when they occurred (breakdown cycles, reopening cycles or after shut-in).

Line 329: “not reached during the break-down cycle”. Why? Do you have an explanations? That is Interesting

Unfortunately, we do not have an explanation for it, and we do not want to expand the discussion towards this topic. We prefer to simply report this observation for future research to address the it.

You comment about the injection volume, but I think you need to comment as well more on Figure 2, which brings very important information, that are not described in the manuscript.
I would add:
“Induced events occur mainly nucleating in time in correspondence of the peak in both injection pressure and rate.” First question here might be: Why we do not observe events later? Also, is there a preference between pressure and volume in inducing seismicity? It looks not.

We do not observe that seismicity only occurs when pressure or rate are at their peaks. In fact the largest seismicity rate occurs somewhat after the peak pressures during breakdown or reopening. However, we agree that it is interesting to state that seismicity rate somewhat depend on injection rate but not on pressure.

We added a statement describing these observations in the manuscript.

"In the HF3 case, instead, events look generating also later with respect to the previously observed vertical propagation. This could be a manifestation of fluid-propagation effects and/or fracturing".
It might help also to plot the injection rate with the seismicity rate, to see what are the minimum levels of the injection to trigger seismicity. Perhaps the results might be combined with Figure 3 or to replace Figure 3.

We do not follow the observation regarding HF3. Post-shut-in seismicity also occurs in the cases of HF1 and HF2. Clearly, seismicity rates and propagation reflects fluid-propagation and fracturing. We feel it is not necessary to additionally comment on this in the text.

Also as mentioned above, injection pressure and rate-dependence of seismicity can be observed from Figure 2 and does not require an additional figure.

Line 337 "(see Doescth...)"

We added the word 'see'.

Line 342: "the impact of considering anisotropy produces variations in the spatially.."

We believe our formulation is more precise.

Figure 5 is neat. Why fractures grow in one direction? Is there a lateral stress gradient factor (see Caffagni et al. 2016, GJI)? Could you plot the direction of sigma H max, to see if there are misalignments?

Currently, we do not have an explanation for the downward or upward propagation. The comparison with the stress field estimates from overcoring is done later in Section 5.2 and Figure 13. Note that it does not make sense to discuss the stress field in terms of sigmaHmax, as the stress tensor is rotated with respect to ground surface or the horizontal.

Line 355-358: An explanation of this tendency could be the "Kaiser effect", as observed for instance in the Cooper Basin, (see Baisch et al. 2009, BSSA). I would include this part with one sentence.

We added a sentence on this.

Line 379: attach "wave" and "forms" (waveforms)

Corrected.

Line 402: remove the second "and"

Corrected.

Line 406: "but also accounting for"

Our formulation is correct.

In eq. 2. Ai is in the Fourier domain (frequency) or in time domain? It is not clear..

We added that it is in time-domain.

Line 412-414: Please, clarify this sentence.

We understand that the reviewer has read the originally submitted version of the manuscript. The updated manuscript addressing comments from Reviewer 2, already addressed this sentence, too.

Line 435: replace “accord” with “agreement”

Changed.

Line 436: replace “Figure 2g-i” (?) with “Figure 10 c”

We are actually referring to Figure 2g-i in this sentence and not to Figure 10c.

Line 438: “even with Mra < -3.5 could be located”. Ok, but what is your uncertainty in that range?

We indicate in the text that these magnitudes were located with an error better than 2 m.

Line 454: “the same source mechanism”

This part was shortened in response to reviewer 2.

Line 457: “it was not...DC mechanism” Where do you shown this behavior?

This part was shortened in response to reviewer 2.

Line 465: “of volumetric expansion, likely due to the fluid-injection..”

This part was shortened in response to reviewer 2.

Line 480: “The direction of propagation of HF3 was different from the other..it propagated downward. HF3.. HF3 also...differently in the instantaneous shut..(ISIP), which decreased with...” “with cycle to stabilize...Figure 12” What do you really want to say? Is this significant or a minor factor which can be removed?

We prefer to keep our formulation. We here only state our observations. We prefer to not comment on their significance although we believe that they are significant as they are consistent throughout all cycles.

Line 485: “deepest measurements (HF1 at 18 m) to…, (HF3 at 8 m).”

Changed as suggested.

Line 490: Please spell “OPTV”, never mentioned earlier.

Changed as suggested.

Line 495: “moved 0.3 m downhole, fluid could be injected in a way that fractures were expected to reopen”

Partially changes as suggested

Line 499: “they may have worked...hydrofracture test, since the injected fluid was able to penetrate… Here I actually would add: “Seismicity starts propagating from the packer but not for the HF3 case”

We prefer to keep our formulation, which we believe is clearer.

Line 501: “consistent with the evidence that..” Please also check. It is “decameters” or “meters”? In the mentioned figures, it looks like it is in meters..

In fact, it is decimetres. We changed this in the text.

Line 502: “The low recovery rate of HF3..either by assuming that the packer acts as a sealer of the created fracture after releasing… , or that fluid flows to the far field...”

We prefer to keep our formulation.

Line 510: “ranked 5/5 and 4/5”..? Please provide a short explanation. Not all of your readers knows the overcoring technique in details as you do.

We added a short explanation.

Line 516: “and the fault planes of the HF induced seismicity”

‘Fault’ is not an appropriate term for fracture at a scale of meters. We prefer to keep our formulation.

Line 523: remove 0 in “090”

Changed.

Line 531: “We have shown that micro-seismic monitoring..has provided essential..to obtain a final stress tensor estimate.”

Changed as suggested.

Line 536: “may be due to fractures initiated.”

Changed.

Line 547: “After the initiation, the fracture gradually re-orients itself to become..to the direction preferred of the principal stress.”

We keep our formulation as it is more precise.

Here you may develop arguments including the pressure gradient. See my comment n. 8

We added a short discussion on asymmetric fracture growth and pressure/stress gradients.

Line 556: remove “Once”

Changed.

Line 558: occurred. This reorientation was not...seismic clouds, and it would seem...”
It would be interesting to know why this did not happen..

We keep our formulation.

Line 561. Did you compute the reduction of sigma n on the foliation plane due to the injection? I expect this to be very low..

The goal of this calculation is to compare σ_n on the foliation plane to σ_3. If the injection pressure is used to compute an effective stress, both quantities would reduce by the same amount. Thus, we do not see how this changes the discussion.

Line 570: “We expect focal mechanisms to be in agreement with the stress field orientation… Hence the variability of the mechanisms, which we observe must be due to..”

The section has changed in response to comments by reviewer 2.

Line 577: “associated to fracture propagation. In our case, the observation of DC.. exclude (1)”
No. I do not agree. Please see my comment n. 10.

Double-couple events – even if not pure and imposed by a tensile component – do require shear motion along the source plane. Such a mechanism is not in agreement with pure tensile fracture opening.

We reworded this sentence to explicitly state that pure tensile fracturing can be excluded for the double-couple events (but not necessarily in general).

Conclusion
At the beginning, please, you should insert a sentence that recall the experiment (shortly), or a bit of context. “An experiment at the GTS has been conducted...with the purpose of…”

We added such an introductory sentence.

Line 590: “system to study the..at spatial scale from decimeters to meters. The workflow which we have implemented with standard seismological tools, such as..joint location by station corrections... For other seismological...their uncertainties (e.g., Kwiatek…). In the present case, micro-seismic...proved to be crucial to combine interpretation in the results of the stress...”

We partially changed the formulation for better clarity.

Line 599: “intervals. Such patterns have an EW strike and dip…”

We keep our formulation.

Line 601: “deviated significantly from the normal to the seismic..”

We keep our formulation.

Line 603: “discrepancy” Among what? Please clarify the two terms of the discrepancy

It is the discrepancy explained in the previous sentence. We reworded the previous sentence to make it clearer.

Line 611: “It is possible that stress..and pressure leak-off effects..influence.. Our observations..surveys conducted in moderately anisotropic rock. A combination of...is essential to obtain a reliable interpretation of the link between stress field and small scale HF growth.”

In this way you use words from the abstract and you close the loop.

We prefer to use an alternative formulation for the conclusion.

Appendix

Eq. 2 is meant to be a sum of the ray path contributions in all the layers that you have considered or not?

We state that it is the entire ray path length.

Line 627: revise “inverse”

Corrected.

Line 633: A verb is missing in the sentence.. Please revise

Corrected.

Line 640: remove the second “becomes”

Corrected.

Eq. 13. You mention cos -1. Did you mean the arccos(x) or the sec(x) =1/cos(x)? Please specify to avoid confusion

We meant arccos and corrected it.

References

ASTM (2008) is missing!

We could not find the reference ASTM (2008) so we changed the citation to Zang and Stephansson, (2010)

Evans et al. It is 2005a or 2005? Please check in the text and revise

We removed the a.

Hollinger et al. You have written in the text “Hollinger”. Please, revise

It should be Holliger. We changed it in the text.

Jeffrey, 2000. Not clear what is it.. a book or a paper?

It is actually a patent. We reference it properly.

Manthei et al. 2003. This reference is missing!

No, it is actually there.

Martinez-Garzon. Please write correctly this surname in the text and reference

We corrected it in the text.

Pine and Batchelor. There is written 2003 but also 1984.. Please revise accordingly

It should be 1984. Corrected.

Rutledge et al. 2004. There is another Rutledge and Phillips, 2004 in the text. Please, revise

Rutledge and Phillips, 2004 was changed into Rutledge et al, 2004 in the text.

Van As and Jeffrey (2000). There is another Van As (2000). Is the same? Please, revise

Van As (2000) was changed into Van As and Jeffrey (2000).

Warpinski et al. The two dates in the references do not match the date in the text. Please, revise

Corrected.

Thomsen and/or Thomson reference is missing! What date then? 1986 or 1989? Please, revise

We added the reference and corrected the year. It is Thomson, 1986.

Figure 3: Is the "Injected volume" a cumulative injected volume? If so, it is better to revise the horizontal label

We corrected it in the caption.

Figure 4: Caption "c) Difference...models. It is shown the station.."

Changed as suggested.

Figure 11: Caption: "agrees with one of the focal planes.."

The figure and caption has changed in response to reviewer 2.

Figure 13: Caption: "Comparison between the foliation plane, fractures….with the seismicity cloud directions..."

We keep our formulation.

On the link between stress field and small-scale hydraulic fracture growth in anisotropic rock derived from microseismicity

Gischig, Valentin S.[1*], *Doetsch, Joseph*[1], *Maurer, Hansruedi*[1], *Krietsch, Hannes*[1], *Amann, Florian*[1], *Evans, Keith F.*[1], *Nejati, Morteza*[1], *Jalali, Mohammadreza*[1], *Valley, Benoît*[2], *Obermann,* ~~*Anne*[1]~~*Anne*[3], *Wiemer,* ~~*Stefan*[1]~~*Stefan*[3], *Giardini,* ~~*Domenico*[1]~~*Domenico*[1]

[1]*Departement of Earth Sciences, ETH Zürich, Switzerland.*
[2]*Centre for Hydrogeology and Geothermics (CHYN), Université de Neuchâtel, Switzerland.*
[3]*Swiss Seismological Service, ETH Zürich, Switzerland.*
**Correspondance to: Valentin S. Gischig (gischig@erdw.ethz.ch)*

Abstract To characterize the stress field at the Grimsel Test Site (GTS) underground rock laboratory a series of hydrofracturing ~~test~~ and overcoring ~~test~~tests were performed. Hydrofracturing was accompanied by seismic monitoring using a network of highly sensitive ~~piezo sensors~~piezosensors and accelerometers that were able to record small seismic events associated with ~~decimeter~~meter-sized fractures. Due to potential discrepancies between the hydro-fracture orientation and stress field estimates from overcoring, it was essential to obtain high-precision hypocenter locations that reliably illuminate fracture growth. Absolute locations were improved using a transverse isotropic P-wave velocity model and by applying joint hypocenter determination that allowed computation of station corrections. We further exploited the high degree of waveform similarity of events by applying cluster analysis and relative relocation. Resulting clouds of absolute and relative located seismicity showed a consistent east-west strike and 70° dip for all ~~hydro-fractures.~~hydrofractures. The fracture growth direction from microseismicity is consistent with the principal stress orientations from the overcoring stress tests, provided an anisotropic elastic model for the rock mass is used in the data inversions. σ_1 is significantly larger than the other two principal stresses, and has a reasonably well-defined orientation that is subparallel to the fracture plane. σ_2 and σ_3 are almost equal in magnitude, and thus lie on a circle defined by the standard errors of the solutions. The poles of the microseismicity planes also lie on this circle towards the north. ~~The trace of the hydraulic fracture imaged at the borehole wall show that they initiated within the foliation plane, which differs in orientation from the microseismicity planes. Thus, fracture initiation was most likely influenced by a foliation-related strength anisotropy.~~ Analysis of P-wave polarizations suggested double-couple focal mechanisms with both thrust and normal faulting mechanisms present, whereas strike-slip and thrust mechanisms would be expected from the overcoring-derived stress solution. The reasons for these discrepancies ~~are not well understood~~can be explained by pressure leak-off, but possibly may also involve stress field rotation around the propagating hydrofracture. Our study demonstrates that microseismicity monitoring along with high-resolution event locations provides valuable information for interpreting stress characterization measurements.

1 Introduction

Hydraulic fracturing (HF) is a method of creating ~~new fractures~~artificial fracture networks in a rock mass by high-pressure fluid injection. It has become an essential technique in many underground engineering activities, including the enhancement of permeability in tight oil and gas reservoirs (Economides et al., 2000; Warpinski et al., ~~1992~~1998), and increasing the productivity of mines by fragmenting ore bodies (Jeffrey, 2000; Van As and Jeffrey, 2000). It is useful to distinguish between hydrofracturing (HF), and hydroshearing (HS~~), which~~). HS is a method of rock mass permeability enhancement that uses fluid injections to elevate pore pressure within the rock mass, thereby promoting the shear failure and attendant dilation and permeability increase of pre-existing fractures and faults that are close to critical stress. The amount of pore pressure increase required to initiate shear failure depends upon the degree of criticality (i.e., proximity to failure) of the discontinuity sets present in the reservoir, and is invariably less than required to drive new hydrofractures (Pine and Batcherlor, 1984; Kaiser et al., 2013). ~~Hydroshearing~~HS is often exploited in ~~deep~~enhanced geothermal ~~projects~~systems (e.g~~.~~., Häring et al., 2008; Evans et al., 2005). Small-volume ~~hydrofracturing~~HF is also utilized in stress measurement (e.g., Haimson and Cornet, 2003; Hubbert and Willis, 1972), and is routinely used in many geological engineering projects where a detailed understanding of the stress state is needed to optimize the design of underground facilities (e.g., nuclear waste storage, gas storage, mining, tunneling, hydro-power facilities, etc~~.;~~.; Zang and Stephansson, 2010). For stress characterization, boreholes are drilled into the rock mass and sections with no pre-existing fractures are isolated with hydraulic packers. After an initial pulse injection test to check the tightness of the packed-off interval, water is injected at a constant rate until the rock breaks down~~; that is,~~, i.e., a fracture initiates at the borehole wall. If the borehole is drilled sub-parallel to a principal stress direction, and ~~there are no complications from~~ deviations due to tensile strength anisotropy are not expected, then ~~an axial fracture~~fluid pressure will tend to initiate an axial fracture at the boreholes wall in the direction of the maximum stress that acts normal to the borehole. Further complications can arise where the minimum principal stress is close to aligned with the borehole axis, and the preferred orientation of fracture propagation is in the plane normal to the borehole axis. In this case, the fracture can rotate from axial to lie normal to the minimum principal stress after propagating a short distance outside the wellbore stress concentration (Warren and Smith, 1985; Evans and Engelder, 1989), or even initiate as a transverse fracture (Evans et al., 1988). Subsequently, constant rate injections are repeated for several cycles to reopen and further propagate the fracture, commonly with periods of venting in between. Injection volumes in these small-scale hydrofracturing applications are usually on the order of 10 – 100 liters (Haimson and Cornet, 2003). The pressure response is closely monitored to accurately record the pressure at which the breakdown occurs, and determine the instantaneous shut-in pressure (ISIP), both of which yield information on the local stress and rock stress conditions. The ISIP is the pressure prevailing once viscous pressure gradients have dissipated~~, and for~~. For small volume treatments of importance here, it can be taken as the pressure required to just hold the fracture open~~. It~~, and is thus interpreted as a direct measure of the minimum principal stress magnitude σ_3.

High-pressure fluid injections, whether intended for hydrofracturing or hydroshearing, are invariably associated with microseismic events (or acoustic emissions). Such induced microseismicity can be used as a diagnostic tool to define the geometry and nature of failure of the individual events, regardless of HF scale (e.g., Ishida, 2001; Falls et al, 1992; Majer and Doe, 1986; Lockner and Byerlee, 1977). For this reason, microseismic monitoring is routinely used for monitoring stimulations of EGS reservoirs (Niitsuma et al., 1999), and more recently in oil and gas fracturing operations (e.g., Caffagni et al., 2016; Warpinski et al., ~~2013~~2012; Maxwell et al., 2010~~).~~). At the other extreme of HF scale, it is also used to study the failure process of rock in laboratory tests (e.g~~.~~., Chitrala, 2013)

During small-scale HFs, the orientation of the seismicity cloud is generally considered indicative of the fracture propagation directions, and thus is assumed to be normal to the minimum principal stress (σ_3) direction. Evidence comes from many small to intermediate-scale experiments in the laboratory and under in-situ conditions. Clouds of acoustic emissions in a salt mine observed by ~~Matthei~~Manthei et al. (2003) indicate the local stress conditions and changes thereof. Majer and Doe (1986) showed in a laboratory field experiments that microseismicity clouds propagate perpendicular to the σ_3 direction. Recently, Chitrala et al. (2010) reported HF laboratory experiments on both isotropic sandstone and anisotropic pyrophyllite. They observed that fracture propagation is controlled by the stress orientation in isotropic rock, while in anisotropic rock the fracture orientation is also influenced by the anisotropy orientation. Similarly, laboratory investigations by Doe and Boyce (1989) showed that the stress orientation defines hydraulic fracture propagation only for a stress field anisotropy ratio $\sigma_1/\sigma_3 > 1.5$. At near isotropic stress conditions the fractures branch more strongly and without a preferred propagation direction, a phenomenom often referred as high fracture complexity (e.g~~.~~., Katsaga et al., 2015). During *large-scale stimulations*, there is a tendency for seismic clouds to develop perpendicular to the minimum principal stress direction σ_3 ~~direction~~, (Häring et al., 2008; Evans et al., 2005) particularly for ~~hydrofracture~~HF operations (e.g~~.~~., Rutledge et al., 2004), although for HS stimulations in crystalline rocks there are many examples where the seismicity cloud is oblique to the σ_3 direction (e.g., Block et al., 2015; Murphy and Fehler, 1986; Pine and Batchelor, ~~2003~~1984), presumably reflecting the complex interplay between stress and the pre-existing fracture population that is suitably-oriented for slip reactivation. Furthermore, individual seismicity clusters within the overall seismicity cloud often strike oblique to the maximum principal stress (Eaton and Caffagni, 2015; Deichmann et al., 2014).

It is widely observed during large injections that most induced earthquakes show a double-couple mechanism, which can be taken to indicate that the seismic energy was produced by slip occurring along pre-existing fractures (Eaton and Mahani, 2015; Guilhem and Walter, 2015; Deichmann et al., 2014). Double-couple mechanisms are also observed during HF treatments (e.g., Chitrala et al., 2013; Ishida, 2001; Dahm et al., 1999), although the primary dislocation mechanism during HF is thought to be tensile fracturing (i.e~~.~~., propagation in mode I or opening mode). Detailed~~,~~ moment-tensor analyses of the seismic waveforms have shown that most induced events involve a predominant double-couple mechanism with relatively few indicating an occasionally strong tensile component (Horálek et al, 2010; Guilhem et al., 2014; Šílený et al, 2009; ~~Martinez~~Martínez-Garzón et al., 2017). The wide-spread observation of dominant shear source characteristics of HF-induced microseismicity has been explained by fluid leak-off into small pre-existing fractures (Dusseault et al., 2011). Because tensile fracture opening is very inefficient in radiating seismic energy, the detected seismicity tends to be produced by slip along fractures adjacent to the growing ~~fracture.~~hydrofracture. Thus, these shear events do not represent fracture growth themselves, but nonetheless serve to illuminate the overall plane of growth of the propagating HF.

Although the relationship between seismicity and HF growth is widely discussed in literature, there are few field-scale observations which investigate the relationship ~~of~~between meter-scale hydrofractures formed during stress tests ~~to~~and the ambient stress conditions~~.~~ (e.g., Zang et al., 2017; López-Comino et al 2017). In small-scale laboratory experiments the stress field is imposed to the samples and is precisely known (Chitrala et al., 2010; Doe and Boyce, 1989). In field cases, it is rare that two independent stress characterization methods are applied, even though this is desirable (e.g., Ask, 2009). For the hydrofracture method, the orientation of σ_3 is usually obtained from the orientation of the induced fracture, either from the azimuth of the trace at the wellbore obtained from imprint packers (Haimson and Cornet, 2003), or very rarely from the geometry of the microseismicity cloud (Zang et al., ~~2016~~2017; Majer and Doe, 1986). While simple fracture mechanical considerations suggest that hydrofractures should propagate in a plane normal to σ_3, in isotropic rock (e.g., Detournay, 2016), this is not necessarily the case for anisotropic rock, where theory and observations are sparse. To our knowledge, there are no published field-scale stress surveys which have combined independent methods to investigate the relationship between fracture growth derived from microseismicity and the stress field in an anisotropic rock mass.

In this study, we report on a microseismicity dataset recorded during three HF tests performed for stress field characterization in an underground research laboratory (i.e., the Grimsel Test Site). Independent stress measurements based on the overcoring method (Zang and Stephansson, 2010) were performed in the same borehole, and yielded comparable stress magnitudes but substantial differences in the orientation of σ_3. First, we describe the monitoring strategy and present the temporal evolution of seismicity in connection with the ~~water injections.~~injection histories. Then, we apply anisotropic hypocenter localization including station corrections, as well as cluster analysis and relative localization. Further, we derive relative event magnitudes and focal mechanisms. The results are ~~interpreted in light of~~then compared to the overcoring stress field observations.

2 Experiment context and study site

2.1 The In-situ Stimulation and Circulation (ISC) experiment at the Grimsel Test Site (GTS)

The hydraulic fractures were created as part of a stress and rock mass characterization program that supports the design of a well-controlled and well-monitored hydraulic stimulation experiment, known as the In-situ Stimulation and Circulation (ISC) project (see Amann et al., 2017 for details). The core of this project is a series of injections of up to 1 m^3 water into pre-existing faults to induce fault slip and fracturing. This is accompanied by an extensive monitoring program including measurements of strain, pressure and microseismicity. The ultimate goal of the experiment is to obtain novel insights into the fault stimulation processes that are essential for the technological development of enhanced or engineered geothermal systems (EGSs) and oil and gas well productivity enhancement. The experiments are performed at the Grimsel Test Site (GTS) in Switzerland (Figure 1) operated by the Swiss National Cooperative for the Disposal of Radioactive Waste (Nagra). The GTS is located at 1733 m above sea level and has an overburden of 400 – 500 m. The ISC experiment was performed between two tunnels (i.e~~.~~., the VE and the AU tunnel), and the injection and monitoring boreholes were mostly drilled from the AU cavern at the southern end of the AU tunnel (Figure 1).

The host rock is the so-called Grimsel Granodiorite (GrGr), which changes into the Central Aar Granite (CaGr) about 50 m north of our experiment volume (Keusen et al., 1989). These rocks are part of the Aar Massive - a conglomerate of Variscan intrusions (age ~300 Ma) - that was later intruded by a network of lamprophyres and aplites around the study site. During the Alpine deformation phase, the magmatic rock body experienced greenschist-grade metamorphosis and developed an Alpine foliation oriented roughly 140°/80° (dip direction / dip). Apart from large-scale faults that are often overprinting metabasic dikes (i.e~~.~~., metamorphose lamprophyres), the rock mass in the experiment volume is exceptionally intact, with only a few fracture sets present giving a net fracture density of 0 – 3 per meter.

2.2 Stress field characterization

Since in-situ stress is the ~~major~~relevant force driving fault slip induced during hydraulic stimulation, it is essential to define the local stress field. Thus, an extensive stress characterization program was performed that included both overcoring and hydraulic fracturing. Overcoring is a so-called stress relief method (e.g., Zang and Stephansson, 2010), during which a probe that measures radial strains and in some cases axial strains is inserted into a 38 mm diameter pilot hole. The hole is then overcored with a 116 mm (inner diameter) core bit thereby relaxing the stresses that prevailed within the rock surrounding the 38 mm diam. pilot hole. These stress-relaxation strains are measured by the probe and recorded. Two different probes were used in the stress characterization program. The first is the USBM probe (~~ASTM, 2008~~Zang and Stephansson, 2010) which measures diameter changes of the pilot hole in three directions, thereby defining the stress-relaxation strains in a plane normal to the borehole axis. Inversion of the strains using the measured elastic constants of the rock cylinder yields estimates of the three independent stress components (2D) in the plane normal to the borehole. The second is the CSIRO-HI probe (Worotnicki, 1993). When this probe is inserted into the pilot hole, glue is extruded~~ that serves~~ to bond an array of 12 axial and circumferential strain gages to the wall of the hole. Inversion of the 12 stress-relaxation strains using the appropriate elastic constants yields ~~estimates~~an estimate for the full 3D stress tensors (i.e~~.~~., six components). A total of 16 overcoring experiments were carried out with 10 USBM and 6 CSIRO-HI probes.

The overcoring and hydrofracturing stress measurements were made in three boreholes. Two boreholes, ~~SBH1~~SBH-1 and ~~SBH3~~SBH-3, were drilled into the rock mass immediately to the south of the ISC experiment, where there are no faults and only a few fractures (0-3- fracture per borehole meters). The goal was to characterize the ~~'far-field'~~local stress conditions that are unperturbed by large-scale faults (i.e~~.~~., several tens of meters away from any fault). The first borehole tested (~~SBH1~~SBH-1) was drilled sub-vertically (oriented 260°/75°) from the upper AU gallery (Figure 1, Table 1). It was intended to align with the best estimate of the sub-vertical principal stress~~, whose axis deviated from verticality~~ towards the direction of the minimum principal stress component as estimated by Pahl et al., (1989) and Konietzky (1995~~).~~), who found that axis minimum principal stress deviates from verticality. Four hydrofractures and three USBM overcoring tests were performed in ~~SBH1~~SBH-1 with the goal of deriving the direction of the sub-horizontal stress components. The second borehole (~~SBH3~~SBH-3) was drilled sub-horizontally (190°/-5°, upwards inclined) towards the south from the AU cavern. Three hydrofracturing, three USBM, and three CSIRO-HI overcoring tests were conducted in this hole with the objective of measuring the sub-vertical stress component (hydrofracturing) as well as obtaining estimates of the full stress tensor (overcoring). A third sub-horizontal borehole (SBH-4, oriented 330°/-5°) was drilled towards NW-NNW from the AU cavern so as to penetrate one of the target fault zones of the ISC experiment. Four hydrofracturing, one HTPF~~,~~ (i.e., hydraulic testing of pre-existing fractures), three USBM, and three CSIRO-HI overcoring tests were performed in this hole with the aim of observing possible systematic stress field changes towards the fault zone. The hydrofracture (HF) tests in SBH-3 and SBH-4 were monitored with a ~~micro-seismic~~microseismic monitoring system (due to technical issues ~~micro-seismic~~microseismic monitoring during HF in ~~SBH1~~SBH-1 was not possible). In this study, only ~~micro-seismic~~microseismic events associated with the HF tests in SBH-3 are reported, as the monitoring layout proved to be ideal for recording high quality data. Results from SBH-4 will be reported in future work. A detailed presentation of all stress field investigations is provided by Krietsch et al., (2017~~), and the~~). The main results are given in Table 1, and will be discussed in connection with ~~micro-seismic~~microseismic observations in Section 5

~~**3 Micro-seismic**~~

Table 1: Orientations of boreholes, fractures at the borehole wall, seismicity clouds, and principle stress orientations.

Dip direction and dip [°]		
Borehole SBH-1	260	75
Borehole SBH-3	190	-5
Foliation plane	145	70
Fracture orientation from imprint packers		
SBH-1, 8 m	158	82
SBH-1, 11 m	200	82
SBH-1, 13m	209	81
SBH-1, 15 m	173	79
SBH-3, 18 m (HF1)	143	71
SBH-3, 13 m (HF2)	139	71
Principal stress orientations		
$\sigma_{1,\ iso}$	141	06
$\sigma_{2,\ iso}$	041	57
$\sigma_{3,\ iso}$	235	33
$\sigma_{1,\ aniso}$	093	37
$\sigma_{2,\ aniso}$	190	10
$\sigma_{3,\ aniso}$	293	51
Seismicity planes		
HF1	180	72
HF2	175	76
HF3	178	69
Clusters	172	69

3 Microseismic monitoring

3.1 Data acquisition

Monitoring microseismicity during meter-scale hydrofracturing requires high-sensitivity sensors. We used piezoelectric sensors similar to those commonly used in laboratory acoustic emission experiments~~.~~ (e.g., Ishida, 2002). They were designed by *Gesellschaft für Materialprüfung und Geophysik* (GMuG) for field deployment (Type GMuG Ma-Bls-7-70). These sensors are highly sensitive in the frequency range of 1 – 100 kHz, with the highest sensitivity at 70 kHz. They do not have a well-defined instrument response due to resonance peaks that depend upon sensor design and local installation to the rock (Kwiatek et al., 2011). Thus, ground velocity or acceleration cannot be derived readily. Because of this, the ~~piezo-sensors~~piezosensors at several locations were combined with calibrated one-component accelerometers (Type Wilcoxon 736T) that have a flat instrument response in the range ~2 Hz - ~~25~~17 kHz.

Formatierte Tabelle

Formatiert: Schriftart: Nicht Kursiv

Formatiert: Schriftart: Nicht Kursiv

The network layout is presented in Figure 1. A total of 28 ~~piezo sensors~~piezosensors were used, 20 of which were clamped to polished rock faces at the tunnel wall. Five sensors were installed in each of the following locations: the VE tunnel (same level as AU cavern), in the staircase linking the AU cavern to the KWO tunnel, in the KWO tunnel, and in the upper AU gallery (16 m above AU cavern). The sensor spacing is around 10 - 15 m. The sensors in the staircase, KWO tunnel, and upper AU gallery (sensors S6 – S20) were installed at blasted tunnel walls, which may have a more pronounced excavation damage zone than the ones (S1 – S5) at the mechanically excavated VE tunnel. At four of these sensor positions, accelerometers were glued to the rock next to the ~~piezo sensor~~piezosensor. Additionally to the 20 sensors, a borehole sensor array with eight ~~piezo sensors~~piezosensors and a sensor spacing of 1 m was deployed in borehole ~~SBH1~~SBH-1 (diameter 101 mm). These sensors were pressed pneumatically against the borehole wall. The borehole sensors are the closest to the end of borehole SBH-3, and have a distance of ~9 m from the HF1 interval. The farthest away from the borehole are the sensors S1 - S5 with distance from 55 – 72 m. Note that only a few events were recorded at sensors with source – receiver distance larger than 30 m.

The sensors were ~~read~~digitized with a 32-channel acquisition system that records signals with 1 MHz sampling rate. Prior to digitization, the signals were high-pass filtered with corner frequencies of 1000 Hz and 50 Hz for the ~~piezo sensors~~piezosensors and the accelerometers respectively. The 32-channel system has a built-in event-detection and localization algorithm. At detection of an event, 32.768 ms (i.e~~.~~., 2^{15} samples) of all traces including ~ 10 ms of pre-signal time are stored. Roughly, six event traces of ~32 ms can be stored per second implying that during some time after the events no further events can be detected and stored~~.~~ (i.e., because the system is occupied with storing the current waveform). This 'dead-time' of about 150 ms after each detected event implies that events occurring within this time cannot be detected and recorded. In case of continuous triggering, this would amount to a data loss of 80%. To be able to also detect events that may fall into this dead-time, and to recover small events not automatically detected, 16 selected channels were additionally recorded with a system that recorded data continuously without automatic event detection. Similar monitoring systems have been used in deep mines where they successfully recorded seismicity with magnitudes down to M_w-4.1 (Kwiatek et al., 2011; Plenkers et al., 2010), and in a recent HF experiment in an underground laboratory comparable to our experiment (Zang et al., ~~2016~~2017).

3.3 Joint hypocenter determination and cluster analysis

To obtain high-resolution event location from the microseismic data, the following workflow proved to be effective.

1. *Localization with isotropic velocity model and event filtering:* P-wave arrivals were manually picked. For this, traces were filtered with a band-pass filter with corner frequencies of 1 and 20 kHz. A first locating attempt assuming an isotropic homogeneous medium model with a P-wave

Formatiert: Mittleres Raster 1 - Akzent 21, Einzug: Links: 0 cm, Hängend: 0.75 cm velocity of 5150 m/s was performed to detect mis-picked first arrivals or events with unstable location solutions. Arrival times with large residuals and events with unstable location solutions were re-examined to ensure that no erroneous signals or phases were picked. Then, the following filtering criteria were applied: I) Arrival time with residuals >400 µs were removed. II) Events with too few arrival time observations were removed. Note that although all events were best detected on the 8-sensor borehole sensor array, ~~it spans~~the array aperture is only 7 m and so an additional three arrival times at other ~~piezo sensors~~piezosensors were required. If these were not available, the event was removed. III) Events for which localization did not converge after 200 iterations were removed.

2. *Deriving best-fit anisotropic velocity model:* With the remaining events, a transverse isotropic P-wave velocity model (i.e~~.~~., based on the weak elastic anisotropy approximation of Thomson, 1986) was determined with a grid search algorithm that minimized the median residual RMS over all events. Thomson's formulation for transverse isotropy is:

$$v_P = v_{P,sym}(1+\delta\sin^2(\theta)\cos^2(\theta)+\varepsilon\sin^4(\theta)) \qquad (1)$$

Here, $v_{P,sym}$ is the P-wave velocity along the anisotropy symmetry axis (usually the minimum velocity) and θ the angle between the symmetry axis and the ray path. The Thomson parameter ε describes the relative increase of the velocity perpendicular to the symmetry axis, and δ defines the angular dependence of velocity (i.e~~.~~., the 'shape' of velocity anisotropy). In our grid-search, we varied the symmetry-axis orientation, $v_{P,sym}$, δ and ε.

3. *Joint hypocenter determination (JHD)* (e.g., Maurer and Kradolfer, 1996). With this method, locations are not determined for each event individually. Instead, all events are jointly determined with a least-squares approach, in which also velocity model parameters and station corrections are computed. The latter denote systematic shifts in travel time arising from an error in sensor locations or geological conditions around the sensor (here for instance a pronounced excavation damage zone) that locally reduce the seismic velocity. The anisotropic JHD approach is described in detail in the Appendix. In our case, only station corrections were included in the inversion. The seismic velocity parameters were not computed as the clustered event distribution did not allow for a stable inversion, and because the velocity model was sufficiently constrained with the grid-search approach of Step 2.

4. *Location error estimation:* To compute the error of the source locations~~, we perturbed~~ due to uncertainties in the manually picked arrival times, we perturbed the arrival times with a randomly distributed value with a standard deviation of 0.04 ms (i.e~~.~~., 40 samples). The perturbed arrival times were used to compute new event locations. Repeating this 1000 times yields point clouds of a statistically representative number of possible event locations scattered around the locations determined from the unperturbed arrival times. Applying principle component analysis to these point clouds results in the three principle directions of the point cloud and the error along these (e.g., 95% quantiles or confidence intervals of the location components along the axes). In

Formatiert: Mittleres Raster 1 - Akzent 21

Formatiert: Mittleres Raster 1 - Akzent 21, Einzug: Links: 0 cm, Hängend: 0.75 cm addition to the above event filter criteria, only events whose largest error axis ~~were~~was smaller than 2 m (i.e.±1 m) were used for analysis of the seismicity cloud geometry.

5. *Cluster analysis:* To better resolve details within the seismic clouds, cluster analysis and relative localization were performed following the approach described by Maurer and Deichmann (1995) or Deichmann et al. (2014). Cross-correlation between the P-waves was performed for all events and all stations to derive the correlation coefficient as a measure of waveform similarity and the corresponding lag time. The correlation coefficient of all stations of one event pair is combined ~~by averaging~~as follows: first we apply the variance stabilizing Fisher transformation to the correlation coefficients, then average all transformed correlation coefficients above a threshold of 0.~~9. The~~85, and finally apply the inverse Fisher-transform. Thus obtained averaged correlation coefficients can be combined in a correlation matrix showing the correlation between all event pairs. Event clusters were extracted using this matrix by assuming that similar events should exhibit similar row-patterns, i.e~~.~~., events that strongly correlate should also correlate similarly with all other events. Events are assigned to a cluster if the correlation between the row-patterns are better than 0.~~92~~98. These parameters were determined by trial-and-error.
6. *Arrival time adjustment:* For the events belonging to the extracted clusters the arrival times were adjusted using the approach suggested by Deichmann & Garcia-Fernandez (1992). At any station, the time-differences between events are optimized by considering the time-lags between each event pair of the cluster. To obtain an absolute time for each station and event, a master event has to be determined, to which all other arrival times are related to. We define the master event to be the one with the most P-wave arrivals. In case several events reached the maximum number of arrivals, the one with the largest median over all wave amplitudes was chosen.
7. *Relative relocation:* The adjusted travel times were used to relocate the events of each cluster using the absolute master event location as start value for the inversion.

4 Results

4.1 Temporal evolution during hydrofracturing

Our event catalogue consists of events from the 32-channel real-time event detection and of events extracted during post-processing from the continuous data recorded for 16 channels. All events were visually inspected to separate false triggers (e.g., electromagnetic high frequency or anthropogenic signals) from seismic signals induced by HF. The injection rate and pressure during the three hydro-fractures labeled HF1 (at 18 m borehole depth), HF2 (13 m depth), and HF3 (8 m depth) in borehole SBH-3 (see Figure 1) are shown in Figure 2 along with the cumulative number of detected events. In total 1161, 482 and 274 events were detected during HF1, HF2, and HF3, respectively. The difference in the number of detected events is most likely explained by the proximity of the sources to the borehole sensor array (9 m, 14 m, and 19 m respectively). These sensors were the most sensitive, possibly due to the lower noise-levels in the borehole~~,~~ (i.e., roughly less than half of the noise-level of the tunnel sensors), and their surroundings bearing a greater resemblance to a full-space than applies to the tunnel-wall sensors. All detected events were at least recorded at the borehole sensor array.

Each HF experiment includes four injection cycles – a breakdown cycle (i.e~~.~~., initiation of the fracture) followed by three fracture reopening cycles. In all three experiments, almost all seismic events occurred during fracture reopening, but only few events were associated with breakdown of the rock~~.~~ ~~As shown in Figure 3, the~~ (similar as reported for HF experiments by Zang et al., 2017). Seismicity rates seem to depend on injection rate, even though injection rate is the same for the breakdown cycle and the first reopening cycles (i.e., 1 l/min) but seismicity rates are not (Figure 2). In contrast, seismicity rates do not depend on injection pressure, because they increase for each reopening cycle while pressure is comparable. Seismicity versus injected volume is explored in Figure 3. The injection volume was smallest for the breakdown cycle (0.5 liter for HF1 and 1 liter HF2 and HF3). Also, during the reopening cycles, very few events occurred during injection of the first 0.5 – 1 liter, after which seismicity rates strongly increased. Apparently, a minimum of 0.5 – 1 liters of injection volume is required to induce detectable seismicity, which was not reached during the break-down cycle. Note that the relative event numbers after shut-in (i.e~~.~~., grey lines) generally increases with every injection cycle; 5 – 10 % of all events occurred during the shut-in period of the second reopening cycle, 10 – 15% after the third reopening cycle.

4.2 Joint hypocenter determination (JHD)

After removing bad quality P-wave arrivals or events based on the aforementioned criteria (Steps 1 and 4 in Section 3.3), only 8% (88 events), 19% (92 events) and 25% (69 events) of all events of HF1, HF2, and HF3, respectively, met the criteria for JHD. The parameters used for JHD are given in Table ~~1~~2. The anisotropic P-wave velocity model (Table 2) agrees well with estimates of seismic anisotropy from active seismic experiments at the GTS (see Doetsch et al., 2017; Vasco et al., 1998; Maurer and Green, 1997). The station corrections computed with JHD for both isotropic and anisotropic velocity models are shown for all sensor positions in Figure 4. In the isotropic case, the station corrections show systematic spatial patterns, as clearly seen for the borehole sensor array (Stations 21 – 28). These systematic distributions mostly disappear if anisotropy is considered. Also, the difference of the station corrections of the two velocity models shows that the impact of considering anisotropy is a change of the station corrections with a spatially systematic pattern. Thus, the station corrections strongly compensate for the angular velocity dependency, when an isotropic velocity model is used.

Table ~~1~~2: Anisotropic seismic velocity parameters used for JHD.

Seismic velocity $V_{P,sym}$ in direction of the symmetry axis	5150 m/s
Thompson parameter ε	0.07
Thompson parameter δ	0.02
Symmetry axis, azimuth	330°
Symmetry axis, dip	20°

Formatierte Tabelle

4.3 Seismicity distribution

The distributions of absolute event locations (derived with anisotropic JHD) are shown Figure 5. For HF1 and HF2, the seismicity clouds grow upwards from the injection locations (colored bars indicate packer intervals). The seismicity clouds show an oblate shape of almost 2 m width and lengths of the other two axes of 3.5 m and 5 m. The seismicity cloud of HF3 shows a downward migration and a slight offset to the injection locations (blue bar). Here, most seismicity is concentrated in a narrower band (< 1.5 m) than for HF1 and HF2. The diameter of the cloud is roughly 5 – 6 m. The orientation of the normal to the seismicity clouds are 0° ± 5° in azimuth for all three clouds, and 17°, 13° and 20° in dip for HF1, HF2, and HF3, respectively. There is a tendency for events that occurred during later injection cycles to be located further away from the injection point as the temporal pattern in Figure 5c-e shows. ~~Clear~~Similar observations were made by Baisch et al., (2009), who interpreted it as the ‘Kaiser effect’. However, clear concentric rings of seismicity expected ~~for~~if seismicity only occurs around the propagating fracture ~~propagation during each cycle~~tip are ~~possibly~~not observed. Possibly these rings are smeared to some degree due to limited location accuracy.

In Figure 6a, we show seismicity locations with the error bars, whereas Figure 6b shows the cumulative distribution functions of the errors along the three axes separately (i.e~~.~~., the 95-percentiles along each axis). The latter includes events whose largest error exceeds 2m, the cut-off limit of 2 m used for Figure 5 and 6a being indicated by the dashed line. About 25% of all located events have error limits > 2m. The median of the two-sided error along the three axes is 0.38 m, 0.72 m and 1.34 m. The orientation distribution of the largest error axis is shown in the stereographic projection (lower hemisphere) in Figure 6c, and indicates a predominant E-W azimuth (actually N100°E) of the largest error direction. Note that this closely corresponds to the direction of the largest extend of the seismicity clouds of HF1 and HF2 themselves, as can also be observed in Figure 6a.

The impact of considering anisotropy and station corrections on the shape and location of the seismicity clouds is illustrated in Figure 7a and b for the case of HF1. The largest differences are seen for locations derived using isotropic and anisotropic velocity models. Specifically, the seismicity cloud migrates towards east and upwards by 1 m on average if anisotropy is accounted for. In contrast, the impact of adding station correction is relatively minor; most events migrate by only a few decimeters. Generally, size and orientation of the seismicity clouds in Figures 7a and 7b do not change significantly in all comparisons; the lengths of the long axes of the clouds change by less than 0.5 m, and the orientations by less than 5°. We conclude that cloud size and orientation for all three HFs are robust results under the given location uncertainties. Nevertheless, considering anisotropy is important for the location of the seismicity cloud.

4.4 Cluster analysis and relative location

We found four clusters of events with highly similar ~~wave forms~~waveforms as shown in Figure 8 for Station 9. In ~~all, 112~~total 140 events out of a total of 249 locatable events were found to group in clusters. The largest cluster, denoted Cluster 1, includes ~~70 events, while the other clusters consist of less than 23 events.~~65 events. Note that each cluster does not necessarily consist of events from one hydrofracture, but may include events from all three hydrofractures, as is the case of Cluster 1. The waveforms in Figure 8 are aligned so that the corrected P-wave arrivals match. The high similarity of the P-waves among clustered events, but also between different clusters, is remarkable. We conclude that the fracturing mechanisms of all three fractures are partially similar, and - as expected from the essentially homogeneous rock mass – also the path effects on the wave are comparable. While the P-waves are very similar, the S-waves vary both in amplitude and arrival time. The differences in arrival times are explained by the differences in locations, i.e~~.~~., an arrival time shift of 0.2 ms corresponds roughly to a hypocenter shift of 1 m. The variable S-wave amplitude compared to the P-wave amplitude possibly indicates that the sources may have a variable contribution of tensile components resulting in different S/P-wave amplitude ratios~~ (Eaton et al., 2014)~~. In our case, observed S/P ratios (i.e., median over all sensors per event) range from 0.4 – 7.9. Based on theoretical considerations by (Eaton et al., (2014) who showed that tensile event have S/P ratios that do not exceed 4.617, we infer that events with large S/P ratios are shear-dominated, whereas those with low S/P ratios may have a significant tensile component. Similarly, Kwiatek and Ben-Zion, (2013) inferred the possible presence of tensile components using energy ratios of S- and P-waves. A more detailed analysis of S/P-wave amplitude ratios would require a better understanding of the spatial sensitivity to P- and S-waves of the piezosensors. This will be done in future work.

The events from each cluster were relocated relative to the master event highlighted in Figure 8. The resulting event distributions are shown in Figure 9. Compared to the absolute locations (i.e~~.~~., from JHD), the ~~events~~clusters form much narrower discs (see also Figure 7c). The large axes of the discs cover nearly the entire area of the JHD-derived seismicity clouds. The orientation of the cluster discs only differs by about 5° in strike from the orientation of the~~ ~~JHD-derived seismicity ~~cloud. However, the cluster-derived locations of HF3 are shifted somewhat closer to the packer interval than the JHD-derived ones.~~clouds. The cluster analysis did not reveal distinct sub-groups of events with geometric characteristics different to the overall seismicity cloud, such as found by Deichmann et al. (2014) and Phillips (2000). Instead, clusters contain events across all three fractures and the entire seismicity cloud, and thus helped confirming and refining ~~and ~~the overall geometry of the fractures instead of resolving structures smaller than the fractures.

4.4 Relative magnitudes

We attempt to characterize the relative source strength by deriving a relative magnitude M_r from the P-wave amplitudes. For that purpose, we adapt the concept used by Goebel et al. (2012) for laboratory event magnitudes, but also account for seismic attenuation of the wave as was suggested by Zang et al (~~2016~~2017):

$$M_r = \log_{10}\left(\frac{1}{N}\sqrt{\sum_{i=1}^{N}(A_i \frac{r_i}{r_0} e^{\alpha(r_i - r_0)})^2}\right) \quad (2)$$

Here, A_i is the maximum P-wave amplitude of the signal in time-domain filtered with a narrow band-pass filter between 3 – 7 kHz, r_i is the source-receiver distance, r_0 a reference distance (here chosen to be 10 m), N is the number of stations with a P-wave observation of the event. The parameter $\alpha = \pi f_0/(Q_P V_P)$ is the frequency-dependent attenuation coefficient, where f_0 is the dominant frequency, V_P is the ~~p~~P-wave velocity, and Q_P is quality factor representing aseismic attenuation. We corrected the amplitude A_i following the strategy of Zang et al., (2017), using the ~~dominant~~middle frequency of the band-pass filter, which is f_0 ~~taken as the maximum in the Fourier spectrum~~= 5 kHz, and Q_P = 30 (~~Hollinger~~Holliger and Bühnemann, 1996). The dominant frequencies (i.e., the maxima in the Fourier spectrum) in our case range from 1 – 10 kHz.

Formatiert: Tiefgestellt

Note that the magnitudes derived with this method have no absolute meaning and indicate source strength only relative to other events. To obtain a rough estimate of the recorded maximum magnitude, we compare theoretical spectra using the source model by Boatwright (1978) with the noise recorded at the accelerometers. Thus, we can roughly estimate an upper threshold of magnitudes of events observed at the accelerometers. Only three events were recorded by the accelerometer at sensor position S8, which is at a distance of each 12.3 m from the source with a poor signal-to-noise ratio of each ~3. In Figure 10a and b, the spectra of the three events are compared with noise spectra (converted to velocity from acceleration time series) typically recorded at S8. At around 2 kHz, the three events slightly emerge above the noise. Deriving absolute magnitudes from spectral fitting is not possible. Thus, we only attempt to derive a rough upper bound of the magnitudes by comparing theoretical source spectra to noise~~.~~ (Figure 10a and b). Considering stress drops 1 MPa~~,~~ (Figure 10a), we observed that the spectra of the three events fall ~~between~~in the band defined by the spectra corresponding to Mw-1.0 and -2.0, which would correspond to source radii of ~~25~~4.3 m and ~~8 cm~~1.4 m, respectively. For a stress drop of 0.1 MPa (Figure 10b) the events fall in the band Mw-4.0 to -3.0. The corresponding source radii are within the range of range from ~~18~~0.3 to ~~56 cm~~0.9 m. Thus, the magnitude of the events that were able to be recorded with the accelerometers (i.e., possibly the largest events in our sequence) is not well determined ~~and~~but possibly lies between Mw-3.5 and -1.5 depending on the assumed stress drop. However, the lower range of predicted source radii on the order of ~~8 – 56 cm is narrower. Maximum source radii of a few~~ decimeters to meter are realistic considering that the hydrofractures span a few meters.

For all other locatable events, an *adjusted relative magnitude* M_{ra} by shifting all relative magnitudes obtained from equation 2 by the amount needed to give a value -2.5 for the largest event, thereby establishing approximate ~~accord~~agreement with the mid-range estimate of magnitude M_w of the event from the accelerometer at S8. The resulting adjusted relative magnitudes are plotted in Figure 2g-i. Evidently, the M_{ra} estimates tend to increase with increasing injection cycle. The sensitivity to weaker events is best for HF1, during which even M_{ra}<-3.5 could be located~~.~~ with an error better than 2 m (Figure 6b). Sensitivity degrades towards HF3, because the distance to the borehole sensor array increases. From Figure 10c, we observe that the three HFs were comparable in terms of magnitudes distributions. The adjusted relative magnitudes M_{ra} cover the narrow range from -3.5 to -2.~~3~~5. The b-values of these sequences are overall quite high (b>2), in agreement with other HF studies (e.g., López-Comino et al., 2017), but are determined only for a narrow magnitude range and is thus uncertain.

4.5 Focal mechanisms

Only a few events showed clear P-wave onsets on sufficient sensors to yield the good directional coverage needed to obtain a usefully-constrained fault plane solution. Some examples are shown in Figure 11. Generally, two groups of events could be found: 1) events with compressive P-wave arrivals along the borehole array (located south of the HFs) and tensile arrivals at most of the sensors above the HFs (in the upper AU gallery), and 2) events with the opposite pattern. In the first group, often a normal faulting or oblique normal faulting ~~mechanism~~to oblique strike slip mechanisms could be fitted. ~~Events from Clusters 1 and 3 could be assigned to this group. The second group consists of events that do not belong to any cluster.~~ A thrust faulting mechanism could be fitted for ~~these~~the events of the second group. In five out of ~~six~~nine cases, a focal plane could be fitted that perfectly ~~(Cluster 1)~~ or closely matched the cluster plane. For ~~one of~~ the ~~Cluster 3~~thrust faulting events this was not possible.

~~For Clusters 1 and 3, we also derived polarizations by stacking the wave-forms of all cluster events. If the events all have the same mechanism, waveform stacking would show reliable polarizations. These polarizations are shown in Figure 11, where we consider the different source locations within the cluster that give rise to slight change in radiation direction. Although the polarization pattern is comparable to the patterns from single events, it was not possible to fit a double-couple mechanism. Currently, we cannot explain the discrepancy. Possibly the mechanisms of the events within the cluster vary (as the variable S/P-wave amplitude ratios also indicate; Figure 8), and thus waveform stacking does not give meaningful polarizations. Another reason may be that there are components of non-double-couple mechanisms affecting the polarization pattern. It is also noteworthy that the normal faulting style observed for Clusters 1 and 3,~~It is noteworthy that the normal faulting style contradicts the stress field observations. As described in Section 5.2, the maximum principal stress σ_1 and σ_3 are sub-horizontal and σ_2 and σ_3 are very close in magnitude suggesting that a thrust fault to strike-slip mechanism is expected. Possibly Note that in many other induced seismicity studies most focal mechanisms were in agreement with the prevailing stress field, with only few events deviating from it (e.g., Baisch et al., 2015; Deichmann et al., 2014). Possibly, in our case, a component of volumetric expansion or a compensated linear vector dipole (CLVD) mechanism modifies the pure double-couple mechanisms (Vavrycuk, 2011), Martínez-Garzón et al., 2017). Volumetric expansion would be consistent with growth of a tensile fracture driven by fluid injection.

The double-couple mechanisms found here are in agreement with many studies that showed that seismicity associated with HF have double-couple sources (Chitrala et al., 2013; Dahm et al., 1999; Nolan-Hoeksema & Ruff, 2001; Ohtsu, 1991). The events are thought to be induced either by pressure propagating into the small pre-existing fractures adjacent to growing HF (e.g. Rutledge and Phillips, 2004) or by stress changes induced around the propagating HF (as suggested by Nolen-Hoeksema & Ruff, 2001). In the latter case, it is expected that the stress field locally rotates and that deviations from the ambient stress field reflected in the focal mechanisms occur. Future analysis of seismicity of similar experiment performed at the GTS may give more insights into this.

5 Discussion

5.1 Differences in HF and seismicity characteristics

The three HF experiments are comparable regarding temporal evolution, seismicity cloud orientation and relative magnitude distributions. Nevertheless, HF3 differed somewhat from the other HFs in that it propagated downwards instead of upwards. HF3 also behaved differently in that the instantaneous shut-in pressure (ISIP) decreased with each cycle to stabilize 1 MPa lower than that of the others, and that the fluid volume recovery was markedly less (Figure 12). Indeed, there is a tendency of last-cycle ISIPs, which are taken as direct measures of minimum principal stress, to decrease from ~9 MPa at the deepest measurement, (HF1, at 18 m) to ~8 MPa for the shallowest, (HF3 at 8 m.). A similar decrease is also present in the breakdown pressures, which were 26.1 MPa for HF1, 25.7 for HF2 and for 23.4 MPa. While these slight differences may not be considered significant, the low volume recovery rate of HF3 is noteworthy. Less than 5 - 15 % of the total injected volume was recovered as opposed to HF1 and HF2, for which it was 60 – 75 %. Low volume recovery rates indicate that a pre-existing permeable fracture network may have been intersected by the propagating HF. The Optical Televiewer (OPTV) images of the hydrofracture intervals shown in Figure 12c indicate that all three were free of pre-existing fractures. However, in case of HF3, a two--centimeter-wide dark band of biotite-rich zones can be observed about 10 – 20 cm further downhole. Upon revisiting the exact same interval 1.5 years later (6 February 2017), it was not possible to reopen any fracture. Only when the packer interval was moved 0.3 m downhole could fluid be injected in the manner ~~of that~~ expected for fracture reopening, with pressures comparable to the initial test. It is also noteworthy that no fracture was detected in the imprint packer survey of the interval that was conducted after hydrofracturing. Although the biotite-bands are oriented parallel to foliation (150°/75°) and not parallel to the seismicity cloud (180°/70°), they may have served as weakness zones that were reactivated during the hydrofracture test because water ~~may have~~ was able to penetrate sufficiently far along the packer seat. This explanation is also consistent with the fact that the seismicity cloud was offset towards south (i.e~~.~~., downhole) by a few ~~decameters~~decimeters (Figure 5a and 9). The low recovery rate could be explained either by the packer sealing of the fracture again after releasing pressure from the interval, or by flow to the far field within the permeable structure accessed by the biotite bands.

5.2 Comparison to overcoring stress measurements

Alongside HF, overcoring surveys were performed in all three boreholes as an independent stress characterization method (see Section 2.2). Out of six CSIRO-HI overcoring experiments, three were judged to have provided high-quality internally-consistent results (Bouffier et al., 2015). One of these obtained at a depth of 9 m in SBH-3 was ~~ranked~~rated good (i.e~~.~~., confidence level 4~~/~~ on a total scale of 5), and the other two at depths of 9.2 m and 14.9 m in SBH-4 were ranked 5/5 and 4/5 respectively. Strain data from these three tests were inverted using two elastic models: an isotropic model and transversely isotropic model (Krietsch et al., 2017). The elastic parameters for the models were constrained using numerical modeling to reproduce the strains recorded during bi-axial tests conducted on the instrumented cores immediately after extraction, and supplemented by laboratory tests. The stress tensors obtained from the inversions are presented in Figure 13~~.~~ (values given in Table 1). If an isotropic elasticity model is used, there is a clear discrepancy between stress field orientations from overcoring and the planes of HF-induced seismicity: for it is expected that σ_3 would be normal to and σ_1 and σ_2 to be parallel to the seismicity plane. However, σ_1 is sub-horizontal and subtends an angle of about 60° with respect to the seismicity plane (poles included in Figure 13). Also, neither σ_3 nor σ_2 is normal to the seismicity plane. For the transversely isotropic model, Krietsch et al (2017) performed inversions for a range of parameter sets and showed that the degree of anisotropy (i.e~~.~~., the ratio of the Young's moduli normal to and in the plane of the foliation) had the greatest influence on the principal stress orientations. Using a ratio of two suggested by laboratory tests, the orientation of σ_1 became ~~090~~90°/35~~°~~,° (dip direction /dip), which is sub-parallel to the seismicity planes. The magnitudes of σ_2 and σ_3 are very close, with a difference of less than 2 MPa. As a consequence, small variations in the assumed elastic parameters produce strong variations of the orientation estimates for σ_2 and σ_3, the solutions for both extending almost completely around the circle normal to σ_1 (half-circle in Figure 13). Thus, uncertainties in the parameters defining the transverse anisotropic model preclude a unique determination of the σ_3 direction. However, the three hydrofractures showed consistent orientations lying along the circle defined by the solutions for the σ_2 and σ_3 orientations. We conclude that σ_3 is sub-horizontal oriented north-south and is ~~still~~ sufficiently smaller than σ_2 ~~so~~ that it defines consistent fracture growth directions. Thus, ~~micro-seismic~~we have shown that microseismic monitoring in this case provides essential information for obtaining a conclusive stress tensor estimate.

Also included in Figure 13 are the orientations of the HF initiated at the borehole wall, as determined from oriented imprint (or impression) packer surveys (IP). Successful imprints of the traces of the induced fractures were obtained only for HF1 and HF2 in SBH-3. The absence of a trace for HF3 may be because the fracture initiated some decimeters downhole of the interval, as mentioned earlier (see Section 5.1). The traces of both fractures have orientations that are close to the foliation plane, which has a markedly different orientation to that of the seismicity clouds. The poles of the fracture traces obtained from imprint packer surveys of the four HF intervals in the sub-vertical SBH-1 borehole are also shown in Figure 13. These fractures scatter within a ±20° range, and match the seismicity cloud orientations on average.

In SBH-3, the foliation and its relative orientation with respect to the borehole may play a role both in influencing near-wellbore stress concentrations and in fracture initiation along the weak direction. The initiation of hydrofractures is controlled by the stress state around the wellbore, which includes a contribution from the steadily-increasing wellbore fluid pressure, and by defects and cracks in the borehole wall. Once a fracture is initiated, it enters a regime in which its growth is dominated by fracture toughness and thus may deviate from local principal stress orientations. After this initial stage, the fracture gradually reorients to become aligned with the direction preferred by the principal stress directions. The reorientation process of hydro-fractures is controlled by many factors including fluid properties, injection rate, or stress field anisotropy (Zhang et al. 2011). Experimental evidence shows that anisotropic behaviour in crystalline rock is often the result of micro-cracks that have a preferred orientation parallel to the foliation plane (Nasseri and Mohanty, 2008). Such a micro-structure can produce anisotropy ratios of elasticity, strength and fracture toughness as large as two (Nasseri et al. 2010; Dai et al. 2013). Possibly, in our case, these micro-cracks have served as defects or weakness zones at which fractures could initiate. It seems that fractures initiated from flaws within the foliation plane, and propagated initially within this plane both radially and around the borehole. ~~Once beyond~~Beyond the toughness-dominated regime, fracture reorientation with respect to the principle stress directions occurred. Since this reorientation was not observed in the seismic clouds, it would seem to have occurred within a few decimetres. Assuming the stress magnitudes to be σ_1 = 13 – 17 MPa, σ_2 = 8.5 - 9.5 MPa and σ_3 = 8.5 MPa ~~(~~as proposed by Krietsch et al, 2017~~),~~, the normal stress on the foliation plane in the far-field of the borehole is σ_n = 8.9 – 9.4 MPa. Thus, despite the small difference between the normal stress on the foliation plane and σ_3, it was easier for the fracture to cut through foliation instead of propagating along the foliation plane.

Another noteworthy feature of our seismicity clouds is the asymmetric growth of the HFs around the injection interval. Dahm et al. (2010) suggested that asymmetric bidirectional fracture growth during injection and bidirectional to unidirectional growth after shut-in may be driven by gradients of in-situ stress or pore pressure. In our case, fractures grow upwards in case of HF1 and HF2 and downwards in case of HF3, which would imply that a presumed stress or pressure gradient would change direction between 13 and 8 m borehole depths. We also observe unidirectional rather than bidirectional growth. Thus, we argue that the mechanism proposed by Dahm et al. (2010) might not be sufficient to explain asymmetric fracture growth in our case. To date, it is not entirely clear why fractures grew in such unidirectional manner.

Formatiert: Englisch (USA)

It has been observed in various studies that fracture propagation in foliated rock can lead to a mixture of tensile failure mechanisms and shear mechanisms (e.g~~.~~., stepped failure geometry) (Debecker and Vervoort, 2009). ~~We observe no evidence~~From our observations we cannot infer or exclude the existence of the tensile failure mechanism. ~~Rather~~However, the focal mechanism solutions observed for only a few events are a mixture of normal faulting (with some focal planes nearly parallel to the seismicity cloud) and thrust faulting.~~ However, from~~ From our stress field estimates, we would expect strike slip (and possibly thrust faulting) mechanisms reflecting slip along optimally-oriented pre-existing fractures that intersect the HF plane. We argue that focal mechanisms are expected to be in agreement with the stress field orientation~~,~~ if the slip direction is governed only by the locally-uniform ambient stress field. Hence the variability of the mechanisms we observe must be due to additional factors. Nolen-Hoeksema & Ruff, (2001) proposed three mechanisms that may produce seismicity during hydrofracturing. 1) tensile fracturing at the tip of the propagating fracture, 2) pressure leak-off into pre-existing fractures that intersect the propagating hydrofracture, resulting in their weakening and shear failure~~,~~ (e.g., Rutledge et al., 2004), or 3) slip along pre-existing fractures near the fracture tip induced by stress perturbations associated with fracture propagation~~.~~ (Martínez-Garzón et al., 2013, Warpinski and Branagan, 1989). In our case, pure tensile fracturing (mechanism 1) can be excluded for the ~~observation of~~observed double-couple events. To explore the other two mechanisms~~ excludes (1). Considering (2),~~, the shear and normal stress acting on the focal planes in Figure 11 (i.e., the red half-circles) were computed using the stress field estimate by Krietsch et al., (2017), and the values plotted in the Mohr-Coulomb diagram shown in Figure 14. It is evident that overpressures of 7 – 9 MPa are able to explain slip along all observed focal planes. Thus, pressure-induced slip resulting from fluid leak-off ~~may~~ (mechanism 2) can lead to diverse focal mechanisms as ~~also more~~it permits structures that are ~~mis~~not optimally-oriented in the stress field ~~can~~to be reactivated. ~~But~~It is also possible that stress field perturbations arising from the propagating hydrofractures (mechanism 3) may additionally promote criticality along these planes, although this ~~cannot explain normal and thrust faulting events in close proximity. The observation~~is not resolved by the present observations. In this regard, the assumption of ~~the latter would seem to indicate severe stress field perturbation around the sources may be involved, as in mechanism (3) above. As the principle stress magnitudes are relatively close in our case (possibly < 5 MPa between σ_1 and σ_3) such stress perturbation may lead to a local change~~stress homogeneity within the study volume inherent in the ~~stress regime. Future work is~~

Formatiert: Englisch (Kanada)

required to reveal the dominant mechanism leading to observed double couple seismicity.shear and normal stress estimates plotted in Figure 14 may well be too simplistic. The presence of stress heterogeneity, either pre-existing or generated during the injections through mechanism 3 could potentially modify these values.

655 *Table 2: Orientations of boreholes, seismicity clouds, fractures at the borehole wall and principle stress orientations.*

Dip direction and dip [°]		
Borehole SBH-1	260	75
Borehole SBH-3	190	-5
Foliation plane	145	70
Seismicity planes		
HF1	180	72
HF2	175	76
HF3	178	69
Clusters	172	69
Fracture orientation from imprint packers		
SBH-1, 8 m	158	82
SBH-1, 11 m	200	82
SBH-1, 13m	209	81
SBH-1, 15 m	173	79
SBH-3, 18 m (HF1)	143	71
SBH-3, 13 m (HF2)	139	71
Principal stress orientations		
$\sigma_{1, iso}$	141	06
$\sigma_{2, iso}$	041	57
$\sigma_{3, iso}$	235	33
$\sigma_{1, aniso}$	093	37
$\sigma_{2, aniso}$	190	10
$\sigma_{3, aniso}$	293	51

Formatierte Tabelle

Formatiert: Englisch (Kanada)

6 Conclusion

~~Our results demonstrate the benefits~~A series of ~~installing~~ HF tests were performed as part of a ~~micro-seismic~~stress characterization survey at the Grimsel Test Site. The installation of a microseismic monitoring system proved valuable for studying the ~~fracture~~HF process on scales of decimeters to meters. The ~~workflow we have~~ implemented workflow illustrates that many standard seismological tools – such as joint ~~locating~~hypocentre location with station corrections, high-precision relative relocations of event clusters with similar waveforms, and focal mechanism analysis – can ~~readily~~ be applied to ~~failure~~seismicity at such scales. For other seismological observables such as magnitudes, more efforts are required to obtain meaningful results and assess their uncertainties ~~(e.g., as done by Kwiatek et al., 2011).~~. In the present case, micro-seismic monitoring during the hydrofracture experiments proved crucial for the combined interpretation of the results of the stress characterization methods. The three hydrofracture operations in the ~~SBH3~~SBH-3 borehole produced three flattened seismic structures that extended from at or close to the injection intervals. The structures had an EW strike and dipped at about 70° to the south. The overcoring strains inverted using an isotropic elastic model yielded stress tensor solutions whose minimum principal stress, σ_3, deviated significantly from normal to the seismic structures, as would be expected if the ~~structures defined the plane of hydrofracture growth~~hydrofractures grow normal to σ_3. The discrepancy could be resolved by using a transversely isotropic elasticity model whose parameters were consistent with laboratory measurements on the core. Imprint packer surveys of the injection intervals in ~~SBH3~~SBH-3 showed that the fractures initiated at the borehole wall within the foliation plane, whose orientation differs significantly from that of the seismic structures. We interpret this to indicate that fracture nucleation occurred on flaws that lay in the foliation plane, and that the fracture initially extended within this weakness plane before rotating to lie normal to the minimum principal stress after propagating at most several decimeters. Focal mechanisms show a mixture of normal faulting and thrust faulting mechanisms, whereas a strike-slip mechanism, or possibly thrust, is expected from the stress field orientation. It is conceivable that stress perturbation and pressure leak-off around the propagating fracture strongly influences the source mechanism of the seismic events. Our observations illustrate the challenges faced in stress characterization surveys in moderately anisotropic rock; a combination of overcoring, HF, and micro-seismic monitoring were essential to arrive at a conclusive interpretation of the all observations.

Acknowledgments

The ISC is a project of the Deep Underground Laboratory at ETH Zurich, established by the Swiss Competence Center for Energy Research - Supply of Electricity (SCCER-SoE) with the support of the Swiss Commission for Technology and Innovation (CTI). Funding for the ISC project was provided by the ETH Foundation with grants from Shell and EWZ and by the Swiss Federal Office of Energy through a P&D grant. Hannes Krietsch is supported by SNF grant 200021_169178. The Grimsel Test

Site is operated by Nagra, the National Cooperative for the Disposal of Radioactive Waste. We are indebted to Nagra for hosting the ISC experiment in their GTS facility and to the Nagra technical staff for onsite support. We also thank G. Kwiatek and E. Caffagni and an anonymous reviewer for their valuable comments and corrections that helped improving the manuscript.

Appendix: Earthquake location using an anisotropic velocity model

In the following, we derive the analytical derivatives used for the Jacobi matrix for earthquake location considering transverse isotropic P-wave velocity. In the joint hypocenter determination, the inverse problem to be solved involves minimizing the discrepancy between the observed and predicted arrival times, that is, $\min\left\{\left\|\mathbf{t}^{\mathbf{obs}} - \mathbf{t}^{\mathbf{calc}}\right\|^2\right\}$ by finding an appropriate set of model parameters

(1) $\mathbf{m} = \left(s_j^x, s_j^y, s_j^z, t_j^0, t_i^S\right)$.

Here, the s_j^x, s_j^y and s_j^z are the hypocentral coordinates of the *j*th event, t_j^0 the source time, and the t_i^S station correction at the sensor position *i*. t_{ij}^{obs} denote the arrival time picks as where the index *i* runs from *1* to the total number of picks N_j, of the event *j*. *j* runs from 1 to the total number of events *M*. They can be collected in a vector $\mathbf{t}^{\mathbf{obs}}$. The predicted travel times t_{ij}^{calc} can be computed as:

(2) $$t_{ij}^{calc} = \frac{l_{ij}}{v} + t_j^0 + t_i^S$$

l_{ij} is the length of the entire ray path between the *i*th sensor and the hypocenter of the *j*th event. The ~~inversre~~inverse problem requires the derivatives $\frac{\partial t_{ij}^{calc}}{\partial s_j^x}$, $\frac{\partial t_{ij}^{calc}}{\partial s_j^y}$, $\frac{\partial t_{ij}^{calc}}{\partial s_j^z}$, $\frac{\partial t_{ij}^{calc}}{\partial t_j^0}$ and $\frac{\partial t_{ij}^{calc}}{\partial t_i^S}$ to be computed.

The partial derivative with respect to the origin time t^0 is

(3) $$\frac{\partial t_i^{calc}}{\partial t^0} = 1 .$$

Similarly, the partial derivative with respect to the station correction t_i^S is

(4) $$\frac{\partial t_i^{calc}}{\partial t_i^S} = 1$$

The derivatives with respect to ($s_j^{x,y,z}$) are computed by considering equation (2). Let us assume that each ray segment l_{ij} is bound the *j*th hypocenter (s_j^x, s_j^y, s_j^z), and the *i*th receiver location ($r_{ij}^x, r_{ij}^y, r_{ij}^z$). The length of a segment is equal to (ignoring the index *j* in the following):

Formatiert: Schriftart: Nicht Kursiv

(4) $$l_i = \sqrt{\left(r_i^x - s^x\right)^2 + \left(r_i^y - s^y\right)^2 + \left(r_i^z - s^z\right)^2}\ .$$

Only the first term of the sum in equation (2) contributes to the derivatives with respect to the hypocentral coordinates (only in the first term the hypocentral parameters (s^x,s^y,s^z) are involved). Unlike in the isotropic case, however, not only the segment l_i contributes to the derivatives with respect to (s^x,s^y,s^z), but also the velocity $v = v(s^x,s^y,s^z)$, which become ~~becomes~~ dependent of the take-off angle of the incoming ray. Therefore, we can write:

(5) $$\frac{\partial t_i^{calc}}{\partial s^{x,y,z}} = \frac{1}{v\left(s^{x,y,z}\right)} \frac{\partial l_i}{\partial s^{x,y,z}} - l_i \frac{\partial v}{v^2 \partial s^{x,y,z}}\ .$$

Here, the derivative in the first term is (considering first s^x):

(6) $$\begin{aligned} \frac{\partial l_i}{\partial s^x} &= \frac{\partial \sqrt{\left(r_i^x - s^x\right)^2 + \left(r_i^y - s^y\right)^2 + \left(r_i^z - s^z\right)^2}}{\partial s^x} \\ &= \frac{-2\left(r_i^x - s^x\right)}{2\sqrt{\left(r_i^x - s^x\right)^2 + \left(r_i^y - s^y\right)^2 + \left(r_i^z - s^z\right)^2}}\ , \\ &= \frac{-\left(r_i^x - s^x\right)}{l_i} \end{aligned}$$

Similarly,

(7) $$\frac{\partial l_i}{\partial s^y} = \frac{-\left(r_i^y - s^y\right)}{l_i}\ ,\ \text{and}$$

(8) $$\frac{\partial l_i}{\partial s^z} = \frac{-\left(r_i^z - s^z\right)}{l_i}\ .$$

The expressions for the spatial derivatives in equations (6) to (8) can also be expressed with angles α_i and β_i that denote the azimuth and the inclination of the ray path leaving the hypocenter. The resulting solid angle ~~is also referred to as~~represents the so-called *take-off angle*.

Equations (6) to (8) can be rewritten in terms of the angles α_i and β_i:

(9) $$\frac{\partial t_i^{calc}}{\partial s^x} = -\cos(\alpha_i)\cos(\beta_i)\ .$$

(10) $$\frac{\partial t_i^{calc}}{\partial s^y} = -\sin(\alpha_i)\cos(\beta_i).$$

(11) $$\frac{\partial t_i^{calc}}{\partial s^z} = -\sin(\beta_i).$$

For the derivative in the second term of equation (5), we have to assume an anisotropic P-wave velocity model. We here use the Thomsen parameterization for weak anisotropy (Thomson, ~~1989~~1986):

(12) $$v = v_{P,sym}\left(1+\delta\sin^2(\theta)\cos^2(\theta)+\varepsilon\sin^4(\theta)\right),$$

where θ is defined as the angle between the symmetry axis of the anisotropic medium, oriented along ϕ^{sym} and the ray segment l_i, oriented along ϕ^{ray}, that is,

(13) ~~$\theta = \cos^{-1}\left(\phi^{sym}\cdot\phi^{ray}\right)$~~ $\theta = \arccos\left(\phi^{sym}\cdot\phi^{ray}\right)$,

with

(14) $$\phi^{sym} = \begin{pmatrix} \cos\phi_{inc}^{sym}\cos\phi_{azi}^{sym} \\ \cos\phi_{inc}^{sym}\sin\phi_{azi}^{sym} \\ \sin\phi_{inc}^{sym} \end{pmatrix}$$

(*inc* = inclination angle, *azi* = azimuth), and

(15) $$\phi^{ray} = \begin{pmatrix} \cos\beta_i\cos\alpha_i \\ \cos\beta_i\sin\alpha_i \\ \sin\beta_i \end{pmatrix}.$$

For determining the derivatives $\frac{\partial v}{\partial s^{x,y,z}}$, we define

(16) $$\Psi = \left(1+\delta\sin^2(\theta)\cos^2(\theta)+\varepsilon\sin^4(\theta)\right),$$

and use the chain rule

(17) $$\frac{\partial v}{\partial s^{x,y,z}} = \frac{\partial v}{\partial \Psi}\frac{\partial \Psi}{\partial \theta}\frac{\partial \theta}{\partial s^{x,y,z}}$$

with

(18) $$\frac{\partial v}{\partial \Psi} = v_{P,sym}$$

(19) $$\frac{\partial \Psi}{\partial \theta} = 2\delta\left(\sin(\theta)\cos^3(\theta)-\cos(\theta)\sin^3(\theta)\right)+4\varepsilon\sin^3(\theta)\cos(\theta)$$

(20) $$\frac{\partial \theta}{\partial s^x} = \frac{\partial}{\partial s^x}\cos^{-1}\left(\begin{pmatrix} \cos\phi_{inc}^{sym}\cos\phi_{azi}^{sym} \\ \cos\phi_{inc}^{sym}\sin\phi_{azi}^{sym} \\ \sin\phi_{inc}^{sym} \end{pmatrix}\cdot\begin{pmatrix} \cos\beta_i\cos\alpha_i \\ \cos\beta_i\sin\alpha_i \\ \sin\beta_i \end{pmatrix}\right)$$

Setting

$$(21)\quad \Gamma = \begin{pmatrix} \cos\phi_{inc}^{sym}\cos\phi_{azi}^{sym} \\ \cos\phi_{inc}^{sym}\sin\phi_{azi}^{sym} \\ \sin\phi_{inc}^{sym} \end{pmatrix} \cdot \begin{pmatrix} \cos\beta_i\cos\alpha_i \\ \cos\beta_i\sin\alpha_i \\ \sin\beta_i \end{pmatrix}$$

$$= \cos\phi_{inc}^{sym}\cos\phi_{azi}^{sym}\cos\beta_i\cos\alpha_i + \cos\phi_{inc}^{sym}\sin\phi_{azi}^{sym}\cos\beta_i\sin\alpha_i + \sin\phi_{inc}^{sym}\sin\beta$$

we can write (considering equation 6 – 11)

$$\frac{\partial\theta}{\partial s^x} = -\frac{1}{\sqrt{1-\Gamma^2}}\frac{\partial\Gamma}{\partial s^x}$$

$$= -\frac{1}{\sqrt{1-\Gamma^2}}\frac{\partial}{\partial s^x}\left(\cos\phi_{inc}^{sym}\cos\phi_{azi}^{sym}\frac{r_i^x - s^x}{l_i} + \cos\phi_{inc}^{sym}\sin\phi_{azi}^{sym}\frac{r_i^y - s^y}{l_i} + \sin\phi_{inc}^{sym}\frac{r_i^z - s^z}{l_i}\right)$$

$$(22)\quad = \frac{1}{\sqrt{1-\Gamma^2}}\left(\begin{array}{l} \dfrac{\cos\phi_{inc}^{sym}\cos\phi_{azi}^{sym}}{l_i} + \\ \left\{\cos\phi_{inc}^{sym}\cos\phi_{azi}^{sym}\dfrac{r_i^x - s^x}{l_i^2} + \cos\phi_{inc}^{sym}\sin\phi_{azi}^{sym}\dfrac{r_i^y - s^y}{l_i^2} + \sin\phi_{inc}^{sym}\dfrac{r_i^z - s^z}{l_i^2}\right\}\dfrac{\partial l_i}{\partial s^x} \end{array}\right).$$

$$= \frac{1}{\sqrt{1-\Gamma^2}}\left(\frac{\cos\phi_{inc}^{sym}\cos\phi_{azi}^{sym}}{l_i} + \frac{\Gamma}{l_i}\frac{\partial l_i}{\partial s^x}\right)$$

$$= \frac{1}{l_i\sqrt{1-\Gamma^2}}\left(\cos\phi_{inc}^{sym}\cos\phi_{azi}^{sym} - \Gamma\cos\alpha_i\cos\beta_i\right)$$

Similarly, we find

$$(23)\quad \frac{\partial\theta}{\partial s^y} = \frac{1}{l_i\sqrt{1-\Gamma^2}}\left(\cos\phi_{inc}^{sym}\sin\phi_{azi}^{sym} - \Gamma\sin\alpha_i\cos\beta_i\right),$$

and

$$(24)\quad \frac{\partial\theta}{\partial s^z} = \frac{1}{l_i\sqrt{1-\Gamma^2}}\left(\sin\phi_{inc}^{sym} - \Gamma\sin\beta_i\right)$$

References

Amann, F.,~~ et al. (~~ Gischig, V., Evans, K., Doetsch, J., Jalali, R., Valley, B., Krietsch, H., Dutler, N., Villiger, L., Brixel, B., Klepikova, M., Kittilä, A., Madonna, C., Wiemer, S., Saar, M.O., Loew, S., Driesner, T., Maurer, H., Giardini, D., 2017~~),~~. The seismo-hydro-mechanical ~~behaviourduring~~behavior during deep geothermal reservoir ~~stimulation~~stimulations: open questions tackled in a decameter-scale in-situ stimulation experiment. Solid Earth Discussions 1–55. doi:https://doi.org/10.5194/se-2017-79.

Baisch, S., Rothert, E., Stang, H., Vörös, R., Koch, C., & McMahon, A. (2015). Continued geothermal reservoir stimulation experiments in the Cooper Basin (Australia). Bulletin of the Seismological Society of America. doi: 10.1785/0120140208.

Baisch, S., Vörös, R., Weidler, R., & Wyborn, D. (2009). Investigation of fault mechanisms during geothermal reservoir stimulation experiments in the Cooper Basin, Australia. Bulletin of the Seismological Society of America, 99(1), 148-158. doi: 10.1785/0120080055

Block, L. V., C. K. Wood, W. L. Yeck, and V. M. King (2015), Induced seismicity constraints on subsurface geological structure, Paradox Valley, Colorado, *Geophysical Journal International*, *200*(2), 1170-1193.

Boatwright, J. (1978), Detailed spectral analysis of two small New York State earthquakes, *Bulletin of the Seismological Society of America*, *68*(4), 1117-1131.

Bouffier, C., F. Lahaie, and P. Bigarre (2015), Stress measurements by overcoring at the Grimsel site, Results from the campaign of August-September 2015*Rep.*, 105 pp, Ground and Underground Risks Department (INERIS).

Caffagni, E., Eaton, D. W., Jones, J. P., & van der Baan, M. (2016). Detection and analysis of microseismic events using a Matched Filtering Algorithm (MFA). Geophysical Journal International, 206(1), 644-658, doi: 10.1093/gji/ggw168.

Chitrala, Y., C. Moreno, C. H. Sondergeld, and C. S. Rai (2010), Microseismic mapping of laboratory induced hydraulic fractures in anisotropic reservoirs, paper presented at Tight Gas Completions Conference, Society of Petroleum Engineers.

Chitrala, Y., C. Moreno, C. Sondergeld, and C. Rai (2013), An experimental investigation into hydraulic fracture propagation under different applied stresses in tight sands using acoustic emissions, *Journal of Petroleum Science and Engineering*, *108*, 151-161.

Dahm, T., G. Manthei, and J. Eisenblätter (1999), Automated moment tensor inversion to estimate source mechanisms of hydraulically induced micro-seismicity in salt rock, *Tectonophysics*, *306*(1), 1-17.

Dahm, T., S. Hainzl, and T. Fischer (2010), Bidirectional and unidirectional fracture growth during hydrofracturing: Role of driving stress gradients, J. Geophys. Res., 115, B12322, doi:10.1029/2009JB006817.

Dai, F., and K. Xia (2013), Laboratory measurements of the rate dependence of the fracture toughness anisotropy of Barre granite, *International Journal of Rock Mechanics and Mining Sciences*, *60*, 57-65.

Debecker, B., and A. Vervoort (2009), Experimental observation of fracture patterns in layered slate, *International journal of fracture*, *159*(1), 51-62.

Deichmann, N., and M. Garcia-Fernandez (1992), Rupture Geometry from High-Precision Relative Hypocenter Locations of Microearthquake Clusters, *Geophysical Journal International*, *110*(3), 501-517.

Deichmann, N., T. Kraft, and K. F. Evans (2014), Identification of faults activated during the stimulation of the Basel geothermal project from cluster analysis and focal mechanisms of the larger magnitude events, *Geothermics*, *52* 84–97.

Detournay, E. (2016), Mechanics of hydraulic fractures, *Annual Review of Fluid Mechanics*, *48*, 311-339.

Doe, T. W., and G. Boyce (1989), Orientation of hydraulic fractures in salt under hydrostatic and non-hydrostatic stresses, paper presented at International Journal of Rock Mechanics and Mining Sciences & Geomechanics Abstracts, Elsevier.

Doetsch, J., ~~H. ~~Krietsch, ~~M.~~H., Lajaunie, ~~C. Jordi, V. Gischig, C.~~M., Schmelzbach, ~~and H.~~C., Maurer, H., Amann, F., (2017~~), Characterizing fractures and~~). GPR imaging of shear zones in crystalline rock~~ using anisotropic seismic inversion and GPR imaging, paper presented at EGU General Assembly Conference Abstracts~~, 9th International Workshop on Advanced Ground Penetrating Radar (IWAGPR). doi:10.1109/IWAGPR.2017.7996074.

Dusseault, M., J. McLennan, and J. Shu (2011), Massive multi-stage hydraulic fracturing for oil and gas recovery from low mobility reservoirs in China, *Petroleum Drilling Techniques*, *39*(3), 6-16.

Eaton, D. W., & Caffagni, E. (2015). Enhanced downhole microseismic processing using matched filtering analysis (MFA). First Break, 33(7), 49-55.

Eaton, D. W., and A. B. Mahani (2015), Focal mechanisms of some inferred induced earthquakes in Alberta, Canada, *Seismological Research Letters*, *86*(4), 1078-1085.

Eaton, D. W., M. van der Baan, B. Birkelo, and J.-B. Tary (2014), Scaling relations and spectral characteristics of tensile microseisms: Evidence for opening/closing cracks during hydraulic fracturing, *Geophysical Journal International*, *196*(3), 1844-1857.

Economides, M. J., K. G. Nolte, U. Ahmed, and D. Schlumberger (2000), *Reservoir stimulation*, Wiley Chichester.

Formatiert: Deutsch (Schweiz)
Formatiert: Deutsch (Schweiz)
Formatiert: Deutsch (Schweiz)
Formatiert: Deutsch (Schweiz)
Formatiert: Deutsch (Schweiz)
Formatiert: Deutsch (Schweiz)

Evans, K., and T. Engelder (1989), Some problems in estimating horizontal stress magnitudes in "thrust" regimes, paper presented at International Journal of Rock Mechanics and Mining Sciences & Geomechanics Abstracts, Elsevier.

Evans, K. F., C. H. Scholz, and T. Engelder (1988), An analysis of horizontal fracture initiation during hydrofrac stress measurements in granite at North Conway, New Hampshire, *Geophysical Journal International*, *93*(2), 251-264.

Evans, K. F., H. Moriya, H. Niitsuma, R. H. Jones, W. S. Phillips, A. Genter, J. Sausse, R. Jung, and R. Baria (~~2005a~~2005), Microseismicity and permeability enhancement of hydrogeologic structures during massive fluid injections into granite at 3 km depth at the Soultz HDR site, *Geophys. J. Int.*, *160*, 388–412.

Falls, S. D., R. P. Young, S. R. Carlson, and T. Chow (1992), Ultrasonic tomography and acoustic emission in hydraulically fractured Lac du Bonnet granite, *J. Geophys. Res.*, *97* 6867–6884.

Goebel, T., T. Becker, D. Schorlemmer, S. Stanchits, C. Sammis, E. Rybacki, and G. Dresen (2012), Identifying fault heterogeneity through mapping spatial anomalies in acoustic emission statistics, *Journal of Geophysical Research: Solid Earth*, *117*(B3).

Guilhem, A., and F. Walter (2015), Full, constrained and stochastic source inversions support evidence for volumetric changes during the Basel earthquake sequence, *Swiss J Geosci*, *108*(2-3), 361-377.

Guilhem, A., L. Hutchings, D. Dreger, and L. Johnson (2014), Moment tensor inversions of M~ 3 earthquakes in the Geysers geothermal fields, California, *Journal of Geophysical Research: Solid Earth*, *119*(3), 2121-2137.

Haimson, B., and F. Cornet (2003), ISRM Suggested Methods for rock stress estimation Part 3: hydraulic fracturing (HF) and/or hydraulic testing of pre-existing fractures (HTPF), *Int. J. Rock Mech. Min. Sci. Drilling*, *40*(7-8), 1011-1020.

Häring, M. O., U. Schanz, F. Ladner, and B. C. Dyer (2008), Characterisation of the Basel 1 enhanced geothermal system, *Geothermics*, *37*, 469-495.

Holliger, K., and J. Bühnemann (1996), Attenuation of broad-band (50–1500 Hz) seismic waves in granitic rocks near the Earth'surface, *Geophysical Research Letters*, *23*(15), 1981-1984.

Horálek, J., Z. Jechumtálová, L. Dorbath, and J. Šílený (2010), Source mechanisms of micro-earthquakes induced in a fluid injection experiment at the HDR site Soultz-sous-Forêts (Alsace) in 2003 and their temporal and spatial variations, *Geophysical Journal International*, *181*(3), 1547-1565.

Hubbert, M. K., and D. G. Willis (1972), Mechanics of Hydraulic Fracturing, *Journal of Petroleum Technology*, *6*, 153-168.

Ishida, T. (2001), Acoustic emission monitoring of hydraulic fracturing in laboratory and field, *Construction and Building Materials*, *15*(5), 283-295.

Jeffrey, R. G. (2000), Hydraulic fracturing of ore bodies, ~~edited~~U.S. Patent No. 6,123,394. Washington, DC: U.S. Patent and Trademark Office.

Kaiser, P. K., B. Valley, M. B. Dusseault, and D. Duff (2013), Hydraulic fracturing mine back trials—Design rationale and project status, in Effective and sustainable hydraulic fracturing, edited, Intech.

Katsaga, T., A. Riahi, D. DeGagne, B. Valley, and B. Damjanac (2015), Hydraulic fracturing operations in mining: conceptual approach and DFN modeling example, Mining Techno*logy*, *124*(4), 255-266.

Keusen, H., J. Ganguin, P. Schuler, and M. Buletti (1989), Grimsel test site: Geology*Rep.*, Nationale Genossenschaft fuer die Lagerung Radioaktiver Abfaelle (NAGRA).

Konietzky, H. (1995), Versuch excavation disturbed zone 3D stress field and 2D disturbed zone modelling for the Grimsel Test Site*Rep.*, Internal Report 95-62. Wettingen: Nagra.

Krietsch, H., V. Gischig, R. Jalali, F. Amann, K. F. Evans, J. Doetsch, and B. Valley (2017), Stress measurements in crystalline rock: Comparison of overcoring, hydraulic fracturing and induced seismicity results, in *ARMA 51st US Rock Mechanics / Geomechanics Symposium*, edited, San Francisco, California, USA.

Kwiatek, G., and Y. Ben-Zion (2013), Assessment of P and S wave energy radiated from very small shear□tensile seismic events in a deep South African mine, Journal of Geophysical Research: Solid Earth, 118(7), 3630-3641.

Kwiatek, G., K. Plenkers, G. Dresen, and J. R. Group (2011), Source Parameters of Picoseismicity Recorded at Mponeng Deep Gold Mine, South Africa: Implications for Scaling Relations, *Bulletin of the Seismological Society of America*, *101*(6).

Lockner, D., and J. Byerlee (1977), Hydrofracture in Weber sandstone at high confining pressure and differential stress, *Journal of Geophysical Research*, *82*(14), 2018-2026.

López-Comino, J., S. Cesca, S. Heimann, F. Grigoli, C. Milkereit, T. Dahm, and A. Zang (2017), Characterization of hydraulic fractures growth during the Äspö Hard Rock Laboratory experiment (Sweden), Rock Mechanics and Rock Engineering, 1-17.

Majer, E., and T. Doe (1986), Studying hydrofractures by high frequency seismic monitoring, paper presented at International Journal of Rock Mechanics and Mining Sciences & Geomechanics Abstracts, Elsevier.

Manthei, G., J. Eisenblätter, and P. Kamlot (2003), Stress measurements in salt mines using a special hydraulic fracturing borehole tool, *PDF). In Natau, Fecker & Pimentel. Geotechnical Measurements and Modelling*, 355-360.

Martínez-Garzón, P., G. Kwiatek, M. Bohnhoff, and G. Dresen (2017), Volumetric components in the earthquake source related to fluid injection and stress state, *Geophysical Research Letters*, *44*(2), 800-809.

Martínez-Garzón, P., M. Bohnhoff, G. Kwiatek, and G. Dresen (2013), Stress tensor changes related to fluid injection at The Geysers geothermal field, California, Geophysical Research Letters, 40(11), 2596-2601.

Maurer, H., and N. Deichmann (1995), Microearthquake cluster detection based on waveform similarities, with an application to the western Swiss Alps, *Geophysical Journal International*, *123*(2), 588-600.

Maurer, H., and U. Kradolfer (1996), Hypocentral parameters and velocity estimation in the western Swiss Alps by simultaneous inversion of P-and S-wave data, *Bulletin of the Seismological Society of America*, *86*(1A), 32-42.

Maurer, H., and A. G. Green (1997), Potential coordinate mislocations in crosshole tomography: Results from the Grimsel test site, Switzerland, *Geophysics*, *62*(6), 1696-1709.

Maxwell, S., J. Rutledge, R. Jones, and M. Fehler (2010), Petroleum reservoir characterization using downhole microseismic monitoring, *Geophysics*, *75*(5), 75A129-175A137.

Murphy, H. D., and M. Fehler (1986), Hydraulic fracturing of jointed formations, paper presented at International Meeting on Petroleum Engineering, Society of Petroleum Engineers.

Nasseri, M., and B. Mohanty (2008), Fracture toughness anisotropy in granitic rocks, *International Journal of Rock Mechanics and Mining Sciences*, *45*(2), 167-193.

Nasseri, M., G. Grasselli, and B. Mohanty (2010), Fracture toughness and fracture roughness in anisotropic granitic rocks, *Rock Mechanics and Rock Engineering*, *43*(4), 403-415.

Niitsuma, H., M. Fehler, R. Jones, S. Wilson, J. Albright, A. Green, R. Baria, K. Hayashi, H. Kaieda, and K. Tezuka (1999), Current status of seismic and borehole measurements for HDR/HWR development, *Geothermics*, *28*(4), 475-490.

Nolen-Hoeksema, R. C., and L. J. Ruff (2001), Moment tensor inversion of microseisms from the B-Sand propped hydrofracture, M-Site, Colorado, *Tectonophysics*, *336*(1), 163-181.

Ohtsu, M. (1991), Simplified moment tensor analysis and unified decomposition of acoustic emission source: application to in situ hydrofracturing test, *Journal of Geophysical Research: Solid Earth*, *96*(B4), 6211-6221.

Pahl, A., S. Heusermann, V. Bräuer, and W. Glöggler (1989), Grimsel Test Site. Rock stress investigations, *Hannover, Germany: BGR-NAGRA Rep. NTB*.

Phillips, W. S. (2000), Precise microearthquake locations and fluid flow in the geothermal reservoir at Soultz-sous-Forêts, France, *Bulletin of the Seismological Society of America*, *90*(1), 212-228.

Pine, R., and A. Batchelor (1984), Downward migration of shearing in jointed rock during hydraulic injections, paper presented at International Journal of Rock Mechanics and Mining Sciences & Geomechanics Abstracts, Elsevier.

Plenkers, K., G. Kwiatek, M. Nakatani, and G. Dresen (2010), Observation of seismic events with frequencies f> 25 kHz at Mponeng Deep Gold Mine, South Africa, *Seismological Research Letters*, *81*(3), 467-479.

Rutledge, J. T., W. S. Phillips, and M. Mayerhofer (2004), Faulting induced by forced fluid injection and fluid flow forced by faulting: An interpretation of hydraulic-fracture microseismicity, Carthage Cotton Valley gas field, Texas, *Bulletin of the Seismological Society of America*, *94*(5), 1817-1830.

Šílený, J., D. P. Hill, L. Eisner, and F. H. Cornet (2009), Non–double-couple mechanisms of microearthquakes induced by hydraulic fracturing, *Journal of Geophysical Research: Solid Earth*, *114*(B8).

Thomsen, L. (1986). Weak elastic anisotropy. Geophysics, 51(10), 1954-1966.

Van As, A., and R. Jeffrey (2000), Caving induced by hydraulic fracturing at Northparkes mines, paper presented at 4th North American Rock Mechanics Symposium, American Rock Mechanics Association.

Vasco, D. W., J. E. Peterson Jr, and E. L. Majer (1998), Resolving seismic anisotropy: Sparse matrix methods for geophysical inverse problems, *Geophysics*, *63*(3), 970-983.

Warpinski, N. R., M. J. Mayerhofer, A. C. Bridges, and J. Du (2012), Hydraulic fracture geomechanics and microseismic source mechanisms, paper presented at SPE Annual Technical Conference and Exhibition, Society of Petroleum Engineers.

Warpinski, N. R., P. T. Branagan, R. E. Peterson, S. L. Wolhart, and J. E. Uhl (1998), Mapping Hydraulic Fracture Growth and Geometry Using Detected by a Wkeline Retrievable Accelerometer Array, in *Society of Petroleum Engineers Gas Technology Symposium*, edited, Catgary, Alberta, Canada.

Warpinski, N. R., and P. T. Branagan (1989), Altered-stress fracturing, Journal of Petroleum Technology, 41(09), 990-997.

Warren, T., and M. Smith (1985), Bottomhole stress factors affecting drilling rate at depth, *Journal of petroleum technology*, *37*(08), 1,523-521,533.

Worotnicki, G. (1993), Comprehensive rock engineering: principles, practices & projects. Volume 3. Rock testing and site characterization, edited, Oxford: Pergamon Press, England.

Zang, A., and O. Stephansson (2010), *Stress field of the earth's crust*, Springer Dordrecht Heidelberg London New York.

Zang, A., O. Stephansson, L.O., Stenberg, K.L., Plenkers, S.K., Specht, C.S., Milkereit, E.K., Schill, G.E., Kwiatek, G.., Dresen, and G.., Zimmermann (2016, G., Dahm, T., and M. Weber (2017), Hydraulic fracture monitoring in hard rock at 410 m410m depth with an advanced fluid-injectionfluidinjection protocol and extensive sensor array, *Geophysical Journal International*, Geophys. J. Int., 208(2), 790–813, DOI:10.1093/gji/ggw430,

Zhang, X., R. Jeffrey, A. Bunger, and M. Thiercelin (2011), Initiation and growth of a hydraulic fracture from a circular wellbore, *International Journal of Rock Mechanics and Mining Sciences*, *48*(6), 984-995.

Formatiert: Englisch (Großbritannien)

Formatiert: Englisch (Großbritannien)

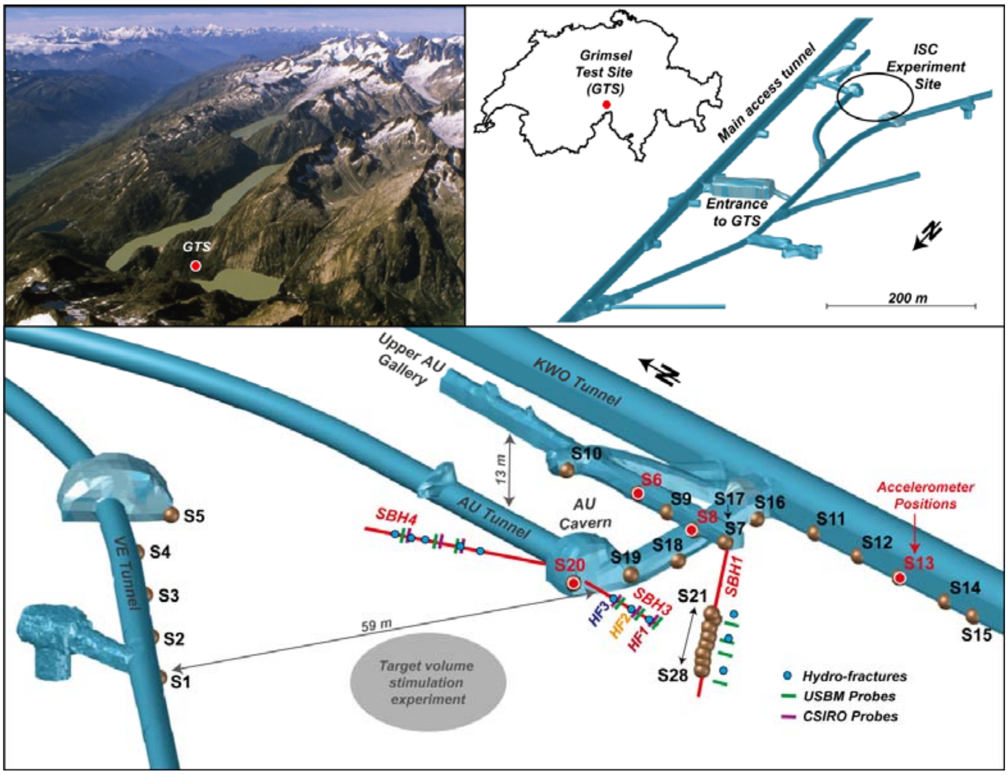

Figure 1: *The study site is located in the Bernese Alps in southern Switzerland (photo from www.grimselstrom.ch/elektrische-energie/kraftwerke-und-stauseen), and consists of a network of tunnels, with the ISC experiment site located between two tunnels. The stress characterization survey used three boreholes (SBH-1, 3 and 4) in which overcoring (using USBM and CSIRO probes) and hydraulic fracturing were performed. S1-S28 mark the seismic sensors.*

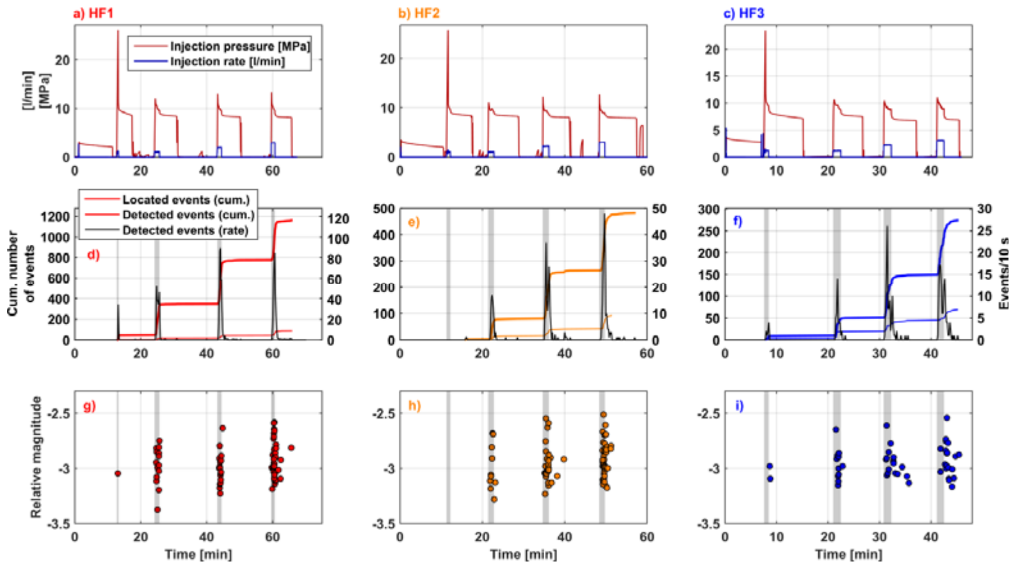

Figure 2: *Temporal evolution of seismic events during hydrofracturing tests in ~~SBH3~~SBH-3. Panels a-c show injection rate and pressure, d-f show the cumulative number of events, and g-i show the adjusted relative magnitude. Events occur mostly during injections (gray shaded areas), but some events occur after shut-in.*

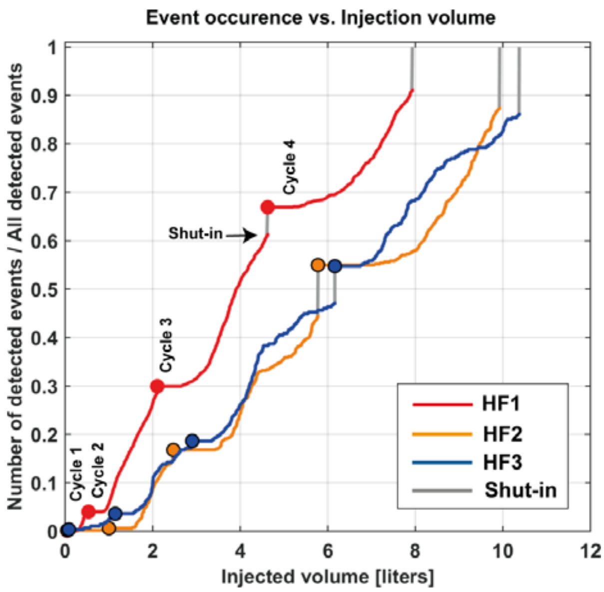

Figure 3: *Cumulative fraction of events as a function of cumulative injected volume for hydro-factures HF1-3.*

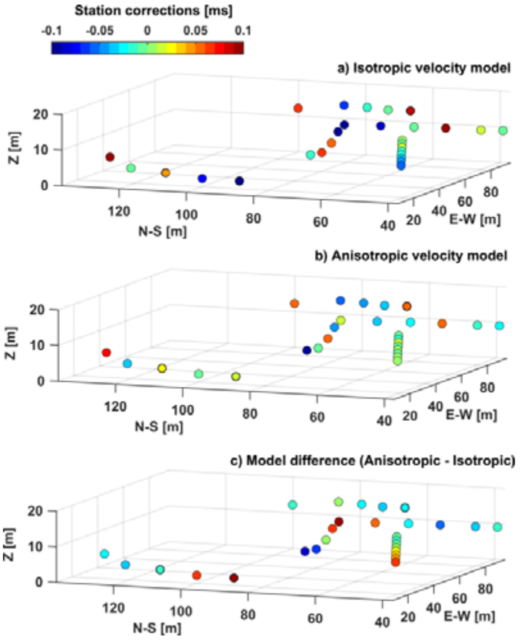

Figure 4: *Sensor distribution and corresponding station corrections. a) Station correction for an isotropic velocity model. b) Station corrections for an anisotropic velocity model. c) ~~The difference~~Difference between station corrections of the two velocity models~~, which~~. It shows the part of the station corrections using an isotropic velocity model that compensates for neglecting anisotropy.*

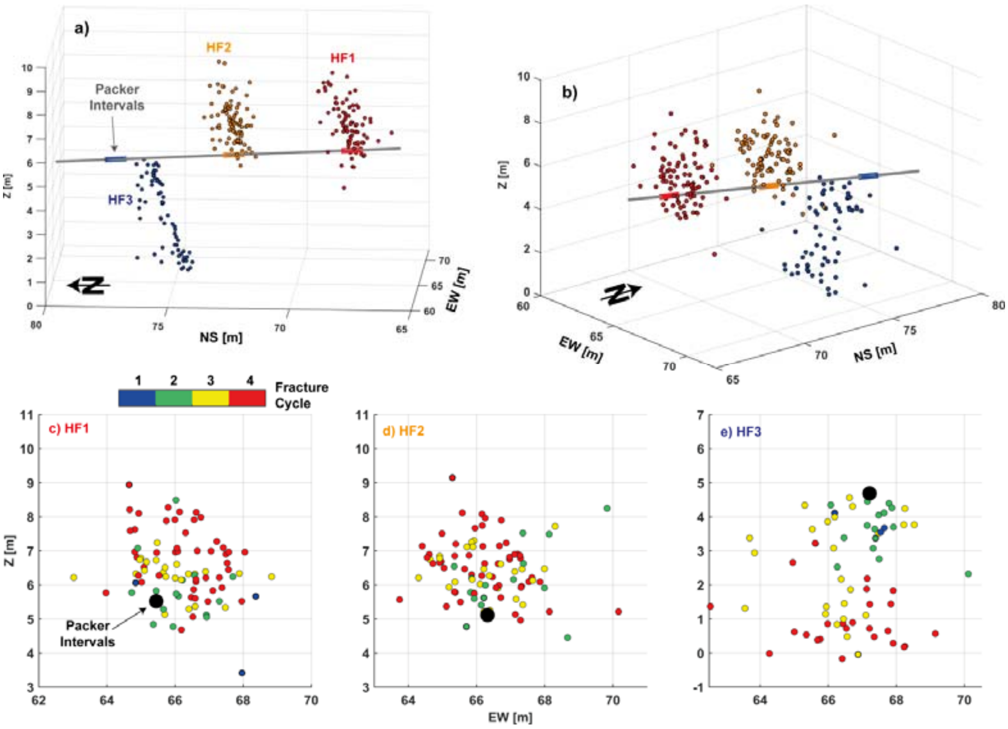

Figure 5: *a) and b) Seismicity clouds of HF1-3 using absolute locations derived from JHD. c) – e) Seismicity clouds (view towards north) with events colored according to the injection cycle during which it occurred.*

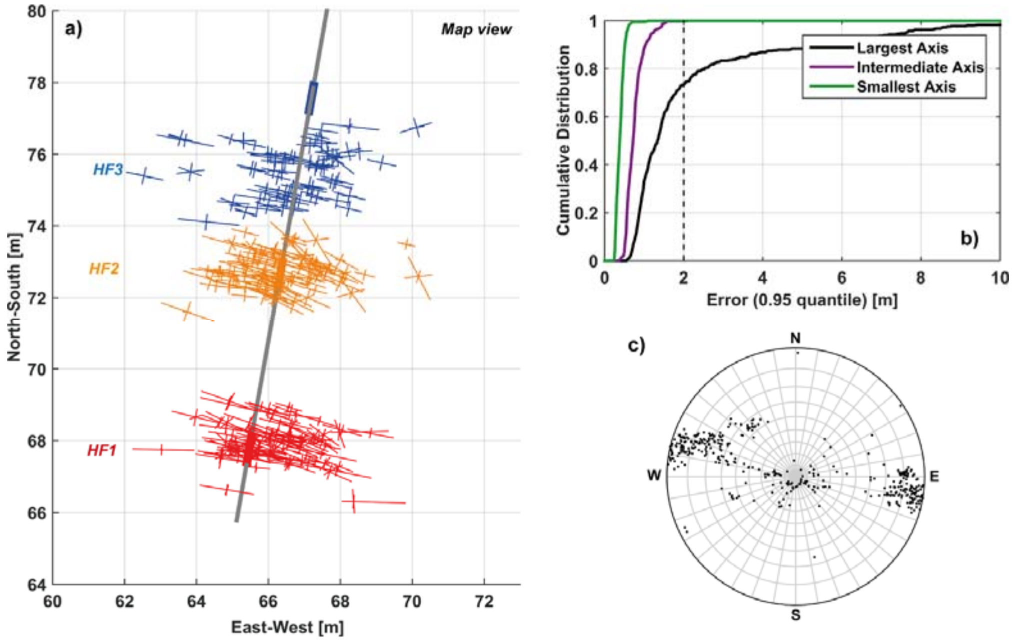

Figure 6: *Error estimates for event locations: a) error ellipsoids shown in map view, b) cumulative distribution of the errors along the three principle axes of the error ellipsoids and c) stereographic projection (lower hemisphere) of the largest error direction. The errors generally are largest in EW direction.*

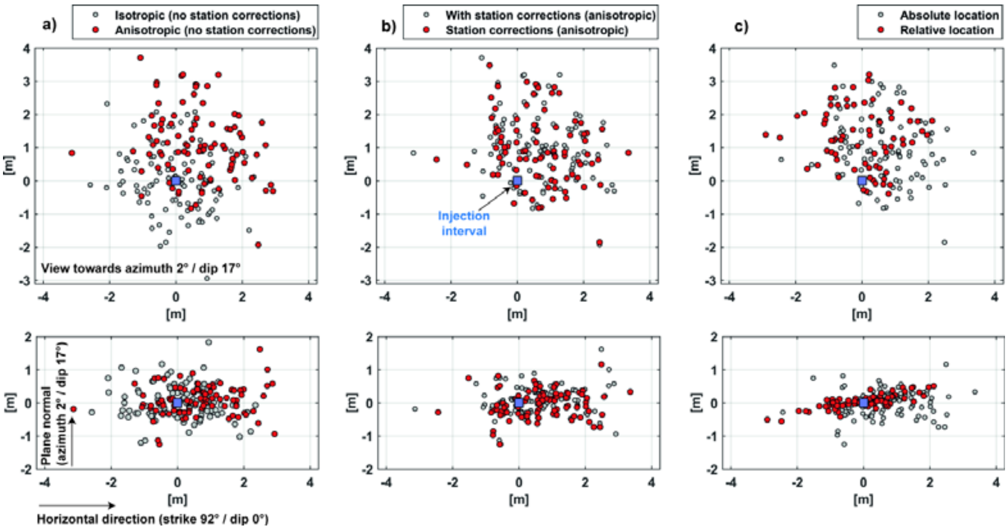

Figure 7*: Impact of anisotropy and station corrections and relative location on source locations. The upper panel is always a projection onto the plane of largest extent of the seismicity clouds. The lower panels are projections perpendicular to -the seismicity cloud. a) Isotropic versus anisotropic velocity models with station corrections not included. b) With and without station corrections for the anisotropic velocity model. c) Absolute versus relative locations for the anisotropic velocity model.*

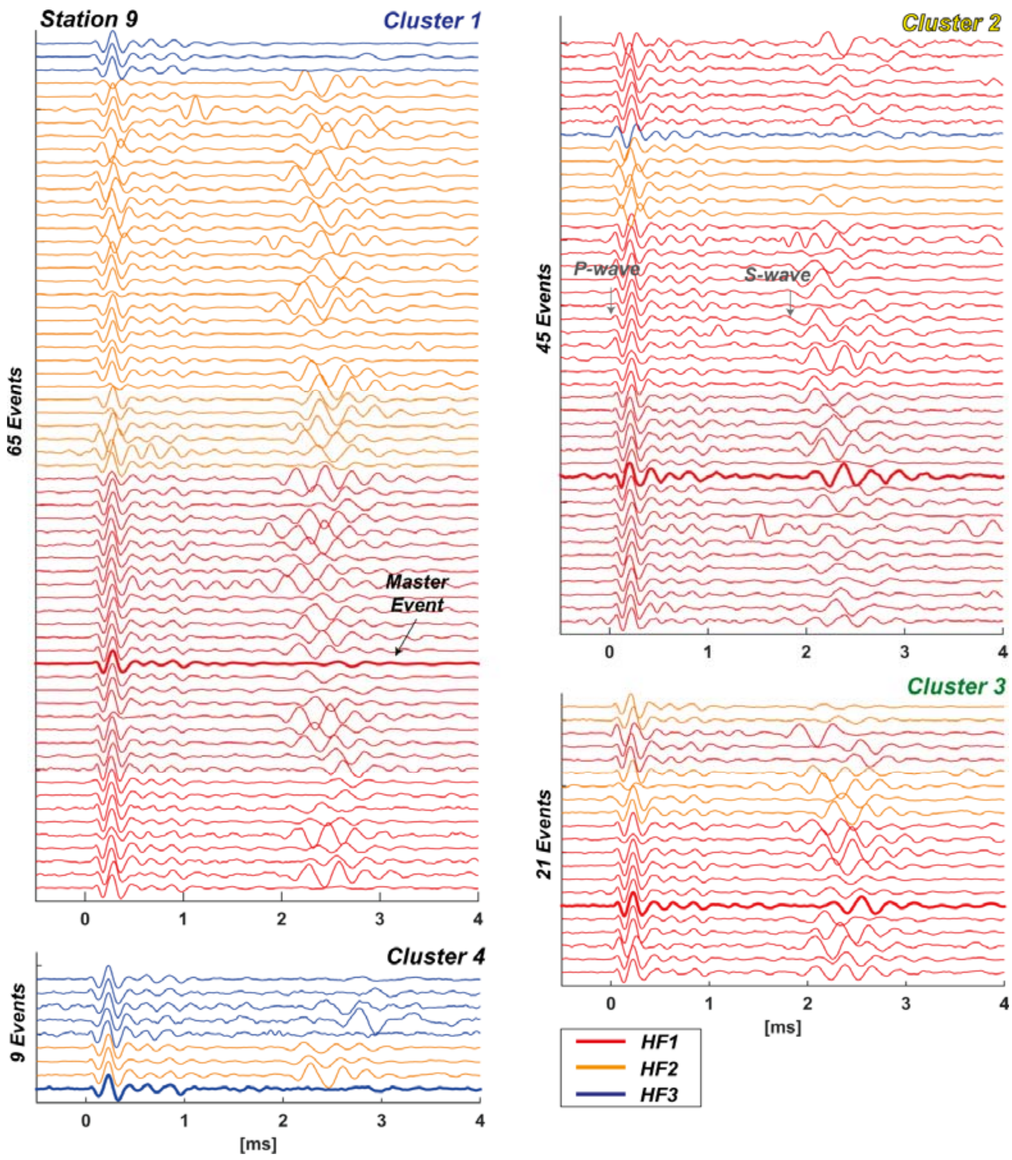

Figure 8: *Selected wave forms events for station S9 and clusters 1-4. Most clusters contain events from several hydraulic fracturing positions.*

1090

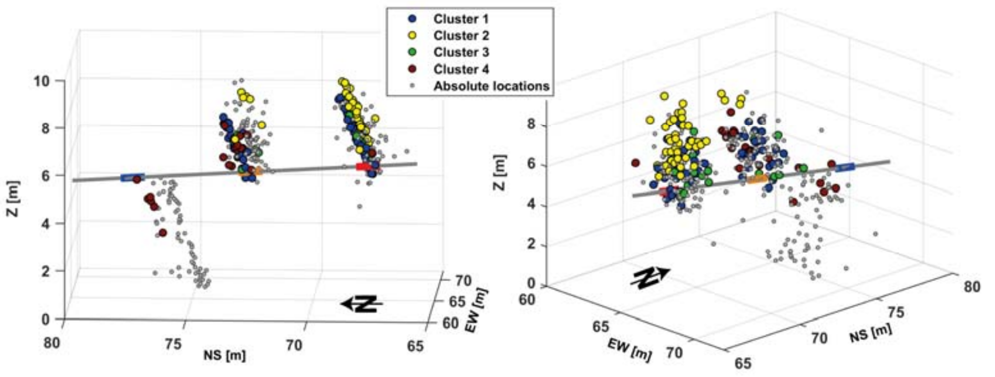

Figure 9: *Relative locations: The hypocentres from relative localization (coloured dots) align along EW planes, with much less scatter than those from absolute localization (grey dots).*

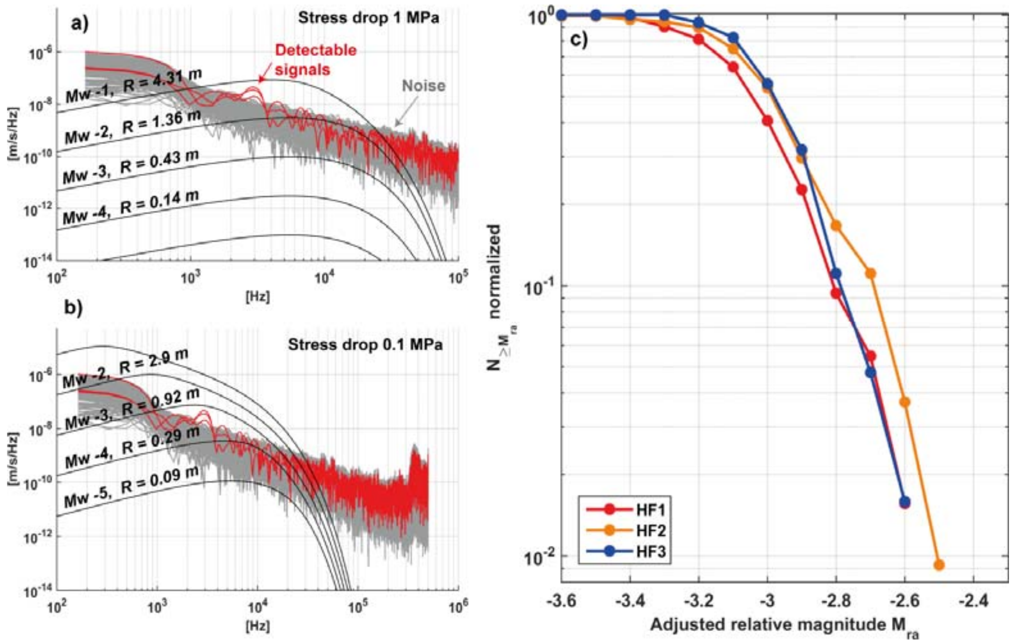

Figure 10: *a) and b) Noise spectra of the accelerometer at sensor position S8 (gray) and the spectra of three events detected at S8. Also shownthe accelerometer (red) slightly emerging above the noise. Superimposed are theoretical spectra for different magnitudes and (Mw -4.0 to -1.0). R denotes the corresponding source radii. The stress drop values.in a) was chosen to be 1MPa, and in b) it was 0.1 MPa. The detected signals (red) fall in the band between Mw -2.0 and -1.0 for a stress drop of 1 MPa and between Mw -4.0 and -3.0 for stress drop of 0.1 MPa. c) Frequency magnitude distribution of relative adjusted magnitudes* M_{ra}.*–These were adjusted so that the maximum magnitude is around* M_{ra}*-2.5 matching a middle value between the approximate maximum magnitude estimates from a) and b).*

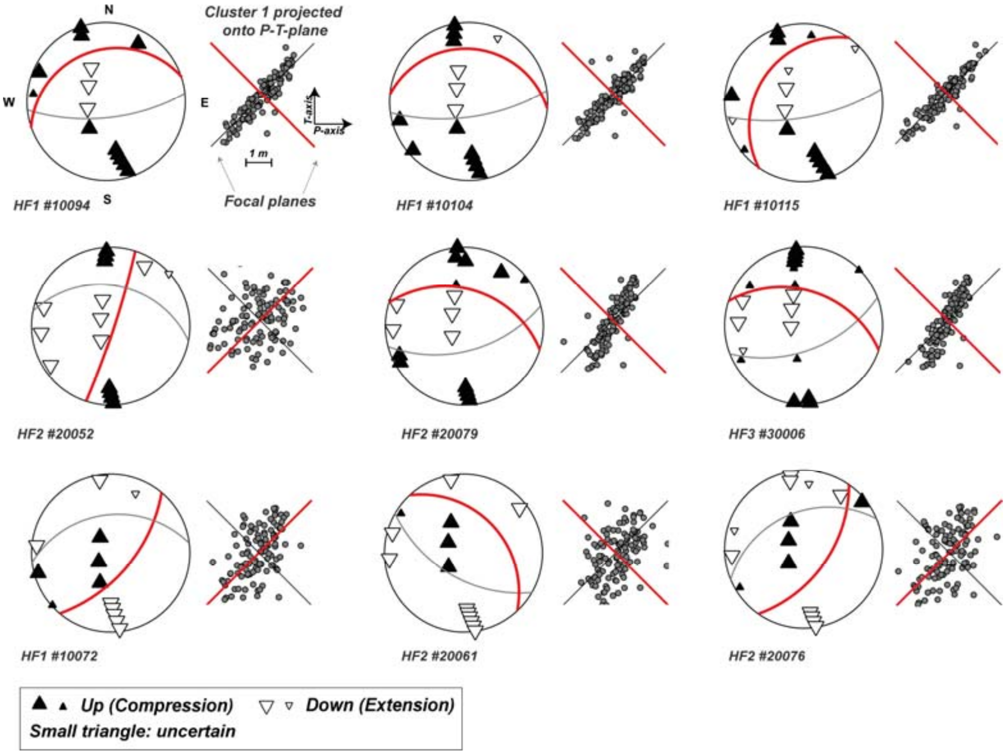

Figure 11: *Stereographic plots of focal plane solutions~~ for a few events.~~, Next to each focal mechanism is the projection of the seismicity cloud of the corresponding ~~hydro-fracture~~hydrofracture onto a plane defined by the P- and the T-axis where the focal planes appear as a diagonal cross. If the seismicity cloud orientation agrees with one the focal planes, the seismic events group closely around one of the planes. Note that the focal plane, on which stress was resolved oin Figure 14, is marked as red line.*

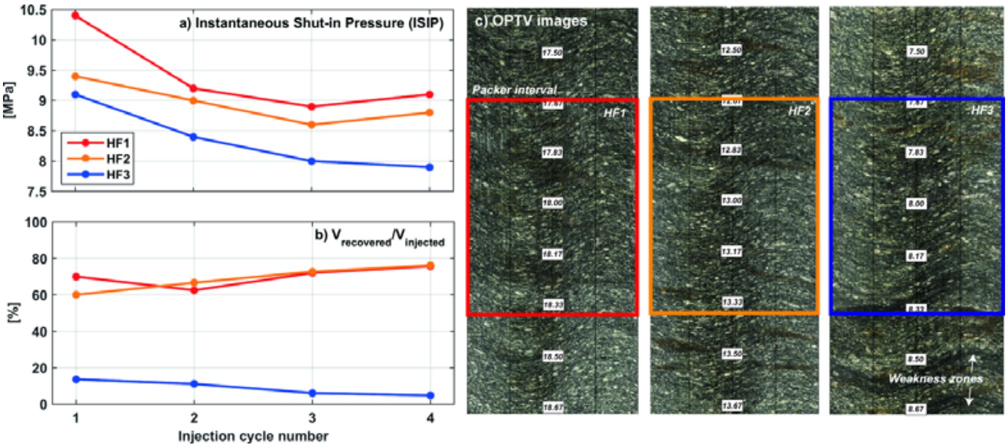

Figure 12: *Hydrofracturing results: a) Development of Instantaneous shut-in pressure (ISIP) and b) relative volume recovery of injected water with cycle for the three hydro-fractures. For HF3, ISIP continues to decrease with each cycle and the recovered volume is very low. c) Optical televiewer images of the three hydrofracturing intervals.*

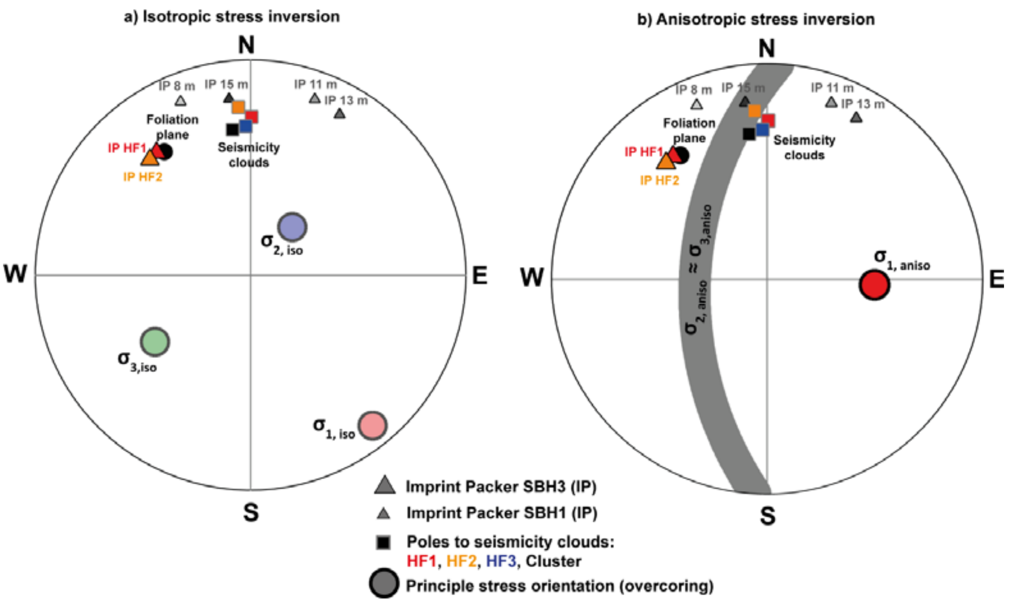

Figure 13: *Comparison of seismicity cloud directions with the foliation plane, fractures mapped on imprint packers (IP) and the principal stress directions from overcoring (σ_{1-3}) with the seismicity clouds. a) For stress inversion of the overcoring assuming isotropic elastic parameters, and b) for transversely isotropic elastic parameters (Krietsch et al., 2017).*

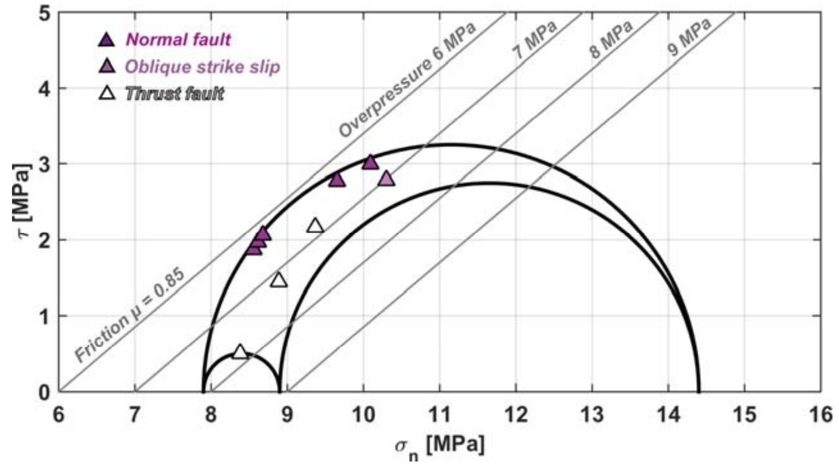

Figure 14: *Mohr-Coulomb diagram representing the stress field estimate by Krietsch et al., (2017) as Mohr circles (including hydrostatic pressure of 0.6 MPa). The failure limits assuming a friction coefficient of 0.85, no cohesion and ovserpressures of 6, 7, 8 and 9 MPa are shown. For the focal mechanisms in Figure 11 the normal stress and shear stress are computed for the focal plane that requires the smallest overpressure (above hydrostatic) to reach failure. All selected focal planes fail for overpressures of 7 – 9 MPa..The focal planes, for which stresses are represented, are indicated in red in Figure 11.*